

Article

Investigating Drought and Flood Evolution Based on Remote Sensing Data Products over the Punjab Region in Pakistan

Rahat Ullah ^{1,2,3}, Jahangir Khan ^{4,5}, Irfan Ullah ⁶, Faheem Khan ^{7,*} and Youngmoon Lee ^{8,*}

- ¹ Jiangsu Key Laboratory for Optoelectronic Detection of Atmosphere and Ocean, Nanjing University of Information Science & Technology, Nanjing 210044, China
 - ² Institute of Optics and Electronics, Nanjing University of Information Science & Technology, Nanjing 210044, China
 - ³ Jiangsu International Joint Laboratory on Meteorological Photonics and Optoelectronic Detection, Nanjing University of Information Science & Technology, Nanjing 210044, China
 - ⁴ Key Lab of Remote Sensing for Agri-Hazards, Ministry of Agriculture, College of Information & Electrical Engineering, China Agricultural University, Beijing 100083, China
 - ⁵ Department of Computer Science & IT, Sarhad University of Science & Information Technology, Peshawar 25120, Pakistan
 - ⁶ College of Hydrology and Water Resources, Hohai University, Nanjing 210098, China
 - ⁷ Department of Computer Engineering, Gachon University, Seongnam-si 13120, Republic of Korea
 - ⁸ Department of Robotics, Hanyang University, Ansan 15588, Republic of Korea
- * Correspondence: faheem@gachon.ac.kr (F.K.); youngmoonlee@hanyang.ac.kr (Y.L.)

Abstract: Over the last five decades, Pakistan experienced its worst drought from 1998 to 2002 and its worst flood in 2010. This study determined the record-breaking impacts of the droughts (1998–2002) and the flood (2010) and analyzed the given 12-year period, especially the follow-on period when the winter wheat crop was grown. We identified the drought, flood, and warm and cold edges over the plain of Punjab Pakistan based on a 12-year time series (2003–2014), using the vegetation temperature condition index (VTCI) approach based on Aqua Moderate Resolution Imaging Spectroradiometer (MODIS) data products. During the year 2010, the Global Flood Monitoring System (GFMS) model applied to the real-time Tropical Rainfall Measuring Mission (TRMM) rainfall incorporated data products into the TRMM Multi-Satellite Precipitation Analysis (TMPA) for the flood detection/intensity, stream flow, and daily accumulative precipitation, and presented the plain provisions to wetlands. This study exhibits drought severity, warm and cold edges, and flood levels using the VTCI drought-monitoring approach, which utilizes a combination of the normalized difference vegetation index (NDVI) with land surface temperature (LST) data products. It was found that during the years 2003–2014, the VTCI had a positive correlation coefficient (r) with the cumulative precipitation ($r = 0.60$) on the day of the year (D-073) in the winter. In the year 2010, at D-201, there was no proportionality (nonlinear), and at D-217, a negative correlation was established. This revealed the time, duration, and intensity of the flood at D-201 and D-217, and described the heavy rainfall, stream flow, and flood events. At D-233 and D-281 during 2010, a significant positive correlation was noticed in normal conditions ($r = 0.95$ in D-233 and $r = 0.97$ in D-281 during the fall of 2010), which showed the flood events and normality. Notably, our results suggest that VTCI can be used for drought and wet conditions in both rain-fed and irrigated regions. The results are consistent with anomalies in the GFMS model using the spatial and temporal observations of the MODIS, TRMM, and TMPA satellites, which describe the dry and wet conditions, as well as flood runoff stream flow and flood detection/intensity, in the region of Punjab during 2010. It should be noted that the flood (2010) affected the area, and the production of the winter wheat crop has consistently declined from 19.041 to 17.7389 million tons.

Keywords: drought monitoring; drought validation; flood impact; GFMS; NDVI; LST; VTCI

Citation: Ullah, R.; Khan, J.; Ullah, I.; Khan, F.; Lee, Y. Investigating Drought and Flood Evolution Based on Remote Sensing Data Products over the Punjab Region in Pakistan. *Remote Sens.* **2023**, *15*, 1680. <https://doi.org/10.3390/rs15061680>

Academic Editors: Ehsan Sharifi and Vincenzo Levizzani

Received: 05 February 2023

Revised: 09 March 2023

Accepted: 13 March 2023

Published: 20 March 2023



Copyright: © 2023 by the authors. Licensee MDPI, Basel, Switzerland. This article is an open access article distributed under the terms and conditions of the Creative Commons Attribution (CC BY) license (<https://creativecommons.org/licenses/by/4.0/>).

1. Introduction

Drought is a complex and creeping hazard because of low annual precipitation, a decrease in soil moisture, and its adverse impact on agricultural, meteorological, ecological, and socio-economic domains worldwide [1,2]. Pakistan is one of the places that has experienced severe drought events from 1871 to 2014, and over the last 50 years, its worst drought was witnessed in 1998–2002, as well as its worst flood in 2010 [3–5]. Pakistan suffers from drought because of a decrease in southwest monsoon rains, which is associated with La Nina and El Nino weather patterns [6,7]. The agriculture sector of the country was affected in the southern region when it was hit by severe droughts in the recent past [8]. During 2000–2001, agricultural growth was severely affected and thus declined. Major crops such as wheat, cotton, and rice productivity were recorded negatively at 10%, while minor crops suffered a severe setback due to long dry spells, and water shortage was up to 51% against the normal 40% [9,10]. Since its inception, the country faced its worst flood in 2010, which affected 24 million people in total, damaged more than 2 million hectares of crops, and incurred 10 billion (USD) in economic losses [11–13].

Pakistan has enough irrigated rivers, such as the Indus, Sutlej, Ravi, and Chenab rivers, which pass through the plain of Punjab [14,15]. The main Indus River flows alongside the west-to-south of the plain, supporting the ecosystems, agriculture, forests, and plains, and is also the key contributor to the region's livelihoods and development [15]. Among all-natural disasters, floods have been reported to be the most common and frequently occurring natural disaster in south Asia over the past many decades, due to environmental and climatic changes, and anthropogenic factors [16–18]. The evidence shows that the region has experienced a global change in monsoon variability, and an enormous increase in the intensity and frequency of the rainfall that has occurred recently [19,20]. The occurrence of these events is more frequent in the south Asia region, where the most densely populated area has shown more uncertainty in the last few decades [21,22]. With a shift to focus on drought indices, pre-requisite probing technologies such as satellite remote-sensing have become crucial, particularly for the timely detection and monitoring of droughts, due to the more prompt availability of spatiotemporal data over the entire globe. Remote-sensing data have been used to monitor meteorological or agricultural drought and flood events to map the composite imagery of the Earth's surface over a variety of different wavelengths [17,23]. To address the stochastic nature of drought and flood, it is necessary to conduct research into several different innovations. These include the development of perfect indices for the monitoring of drought and flood, as well as multivariate indices that can be used to frame the extreme concurrent changes that occur on land, which also can be used to model these changes [23,24].

Recent advances in the meteorological, agronomic, and hydrological aspects of drought have been greatly aided by drought indices' flexibility. Many drought indices, such as the temperature vegetation dryness index (TVDI), water deficit index, crop water stress index, and vegetation temperature condition index (VTCI), have been defined for quantification and near-real-time monitoring with spatial drought extents [25–27]. In the United States of America, drought conditions are measured by the Palmer drought severity index (PDSI), Palmer hydrological drought index, Palmer modified drought index, and Palmer z-index [28]. For long-term drought quantification, the PDSI is a valid tool because it can quantify relative wetness and dryness by using data on temperature and precipitation [28]. Within reasonable limits, time and space comparisons of drought severity are possible under the prevailing meteorological conditions, through quantities such as the standardized precipitation index (SPI) [29–31]. In 2011, Dai et al. investigated the sensitivity of hydro-meteorological indices, such as the SPI and PDSI, to aridity changes in the present and past, pinpointing the most persistent issues and inspiring new forms of the PDSI that show distinguishable occurrences of soil wetness and drought [32,33].

Furthermore, Wu et al. [34] incorporated the Microwave Scanning Radiometer into the Earth Observation System (AMSR-E) for flood monitoring over the region of the Huaihe River Basin China, and validated the water surface fraction (WSF) values with

Moderate Resolution Imaging Spectroradiometer (MODIS) data. To estimate the WSF, which is based on a ratio (wet soil–dry soil), dry soil and wet soil are considered to be the emissivities of the observed dry and wet soils, respectively. Furthermore, Bowling [35] investigated the Special Sensor Microwave/Imager (SSM/I) brightness temperature (TB) data during the summer rain and flood time in southern China, for flood monitoring to derive the SSM/I's atmospheric and hydrological parameters, and also to retrieve the geophysical parameters of the hydrological cycles of the Earth (i.e., rainfall frequency) [35]. In the mid-western U.S., during the summer (of 1993), the scattering index (SI) was applied to determine the flood. This led to record flood levels along the Mississippi River [36]. Tanaka et al. [37] utilized the SSM/I's data over the Mekong Delta lower land of Tonle Sap for the flood–drought cycle (i.e., practical applications in flood monitoring). This presented that the metrological and remote-sensing indices are very promising for rainfall and flood detections.

Shahzaman et al. [9] utilized the normalized difference vegetation index (NDVI) for rainfall monitoring and estimating weather impacts in South Asia. Ali et al. [38] employed AMSR-E and MODIS during 2010 with heavy rainfall and flood to determine the soil moisture or wetness in the contiguous province of Sind (Pakistan), in the south of the Punjab Plain (our study area). They reported that the results of the soil moisture from the MODIS NDVI and the land surface temperature (LST) data were in good agreement with the AMSR-E soil moisture product [39–41]. This proved the effectiveness of high-resolution products in the optical range to determine flood events in the form of heavy rainfall and flood during 2010. This indicated that the employment of NDVI and LST is in line with our MODIS VTCI approach. Furthermore, Han et al. [42] employed the MODIS data products of LS and NDVI to investigate the soil moisture for the greater Changbai Mountains, utilizing the TVDI, which used the wet-edge and dry-edge relationships to reveal temporal changes in the land surface soil moisture conditions. In addition, the understanding obtained from this study will be to generate and distribute the global decadal scale coarse spatial resolution land products derived from the MODIS and Tropical Rainfall Measuring Mission (TRMM), as well as the TRMM Multi-Satellite Precipitation Analysis (TMPA) satellites, with high-quality resolution to monitor the land cover changes vigorously.

With this aim, this study addresses newly identified quality standards and formative notions in remote sensing, as well as obtaining new and timely results. For the winter wheat crop season, it is specifically intended to identify droughts, warm and cold (WAC) edges, and the flooding of rain-fed and irrigated regions. The VTCI approach has been considered in our study to investigate the drought during 2003–2014 and the flood during 2010. Additionally, to explore the region with associated events, VTCI is used to settle on the dry and wet conditions, as well as the Global Flood Monitoring System (GFMS) model for the flood detection/intensity and stream flow during the year 2010 over Punjab, Pakistan. Overall, in the year 2010, flood events demonstrated flood time, duration, and intensity, utilizing the MODIS VTCI imagery (VTCI time series values) from 2010 over the plain of Punjab, which was in good agreement with the precipitation anomalies of the TRMM and TMPA satellites' observations. The utilized MODIS, TRMM, and TMPA data products illustrate the flood events in the region vigorously and revolve around significant and insignificant drought and flood conditions, with all the calculations for the year 2010 crop seasons. This shows that the real-time TRMM flood events are in considerable agreement, with a high accuracy for the determination of flood events in the region. The validations showed that the VTCI drought during 2003–2014 and the flood during 2010 are quite promising.

2. Materials and Methods

2.1. Study Area

The climate of Pakistan is generally dry/warm temperate, and climatic variations prevail from the northern mountains to the south. The climate of the study region, which is located in Punjab, is dry. Annual precipitation ranges from 100 to 600 mm in the south to 1000 mm in the northeast. The Rabi season precipitation ranges from 200 to 500 mm, but can exceed 800 mm in the north during times of heavy rainfall [4,43]. There is a lack of reliable and complete data and proper information network systems, and a lower availability of weather stations, especially in the south Asia region [44]. The severe droughts in Pakistan occurred in the northwest in 1902 and 1951, and in the southeast in 1871, 1881, 1899, 1931, 1947, and 1999. Additionally, it is revealed that the continent's worst drought occurred in 1952, while the longest drought duration was documented between 2000 and 2002 [8]. The plain has a semiarid and semi-humid climate, rendering it prone to spring and summer droughts, due to unpredictable precipitation. Therefore, regional agricultural studies throughout entire seasons depend on the monitoring, prediction, and assessment of the impact of droughts on crop productivity.

For the 1998–2002 severe droughts and the 2010 flood that are on record, their impacts on the region are defined as (23.57–37.07°N, 60.46–77.08°E) for Pakistan and (27.41–34.02°N, 69.15–75.23°E) for this calculation in the region of Punjab Pakistan. In this study, a 633 × 754 km² region of Punjab land was selected to identify and validate the agricultural drought and flood over the region, positioned over plates h23/v05, h24/v05, and h23/v06, as shown in Figure 1.

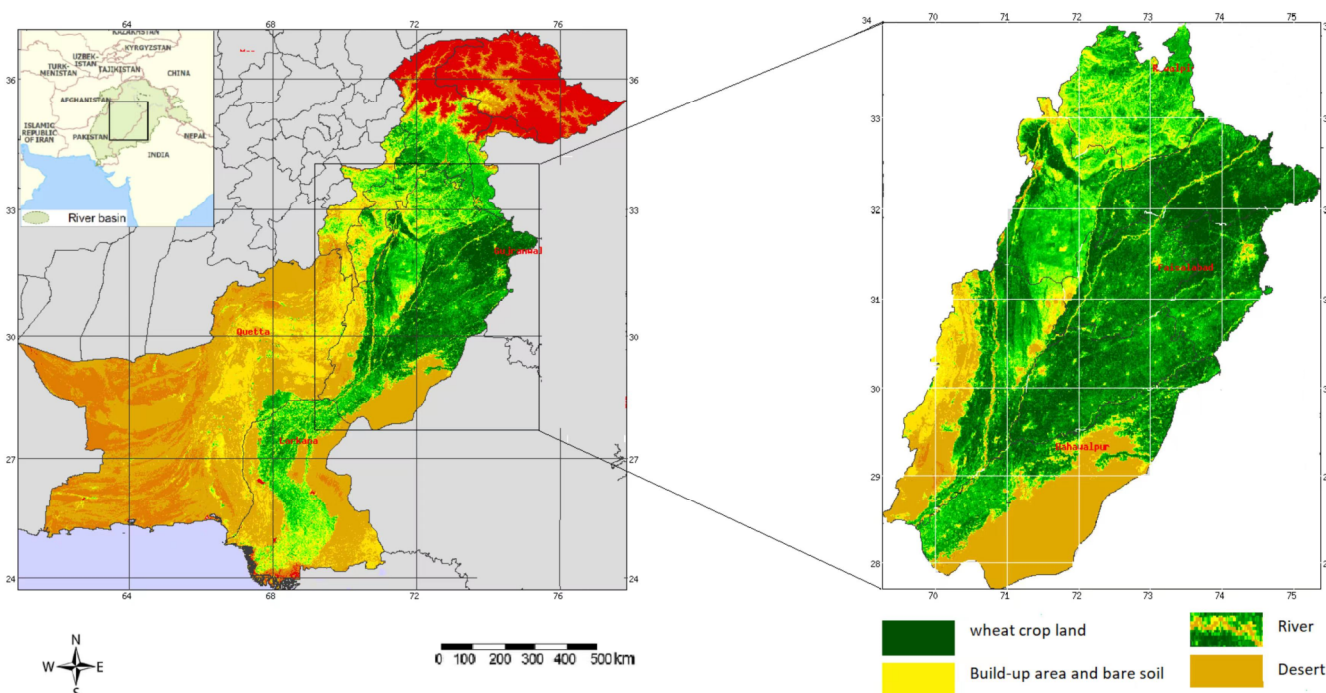


Figure 1. The geographic location of Pakistan and the selected study region representing wheat cropland, rivers, build-up area, bare soil, and desert spread over h23/v05, h24/v05, and h23/v06 plates, defined as (27.41–34.02°N, 69.15–75.23°E) over the region of Punjab Pakistan.

2.2. Datasets

In the current study, we used the Aqua MODIS L3 data products of the 8-day 16 LST (MYD11A2), with bands 31 (10.780–11.280 μm) and 32 (11.770–12.270 μm) as emissivities, and 16-day NDVI (MYD13A2), with bands 1 (red, 620–670 nm) and 2 (near-infrared, 841–876 nm) as emissivity products, using a sinusoidal grid with approximately 1 km. Hence, the land product (grid and pixel size for the 1 km integerized sinusoidal grid is exactly

926.62543305 m) overlaps the h23/v05, h23/v06, and h24/v05 tiles in the in-tegerized, integrated sinusoidal projection, which was assessed in 2014 and located at <https://modis.gsfc.nasa.gov/>, accessed on 20 December 2022. This reprojects the sinusoidal projection to be mosaicked together with a sphere radius ($r = 6,371,007.181$ m), coordinated in the central latitude of 30.0 and central longitude of 75.0 degrees east for the consideration of the study area of Punjab.

The VTCI values that establish the amount and distribution of the vegetation on the land surface fluxes are approximations provided by the included MODIS Aqua data, like the selected bands for LST and NDVI. Band 1 is red (620–670 nm) and Band 2 is near-infrared (841–876 nm), whereas Band 31 and Band 32 are emissivity bands that are used to identify dry and wet areas, respectively, based on their respective wavelengths and descriptions [45]. For exploring drought and warm and cold edges (LST_{max} and LST_{min}), and incorporating flood detection in terms of time, duration, and intensity in the year 2010, we opted for the composite LST-NDVI 16-day data that were achieved from the MODIS Aqua data, and recorded during the winter wheat crop seasons of 2003–2014. In addition to MODIS, the TRMM and TMPA satellites, with high-quality spatial and temporal resolution observations, were used to conclude the land cover changes vigorously. The TRMM (NASA and the Japan Aerospace Exploration (JAXA) Agency joint mission) contributed 17-year (November 1997 to April 2015) datasets on global precipitation and lightning for measuring rainfall events, floods, drought, and weather extremes. The overall system is referred to as the real-time TRMM Multi-Satellite Precipitation Analysis (TMPA-RT). This dataset is the output from the TMPA 3B40RT, 3B41RT, and 3B42RT, and provides precipitation estimates in the TRMM regions that have the (nearly zero) bias of the TRMM (satellite 3B43), combined with instrument precipitation estimations and the dense sampling of high-quality microwave data, with fill-in using microwave-calibrated infrared estimates with a granule size of 3 h.

The daily precipitation data studied for the five stations, with three climatic divisions, were obtained from the Pakistan Meteorological Department (PMD) in the same time period as that of the NDVI and LST. Furthermore, the daily measured precipitation data were deployed for validating the VTCI imageries' values over the five weather stations in a geospatial method, spanning 2002–2014. The VTCI values of the past precipitation, from days to a year, were based on the relationship of departure from normal precipitation (DPNP). For the validation of the VTCI imageries in the specified period, over the southern, central, and northern areas of the plain, we proposed a geospatial NRTC approach during the period of 2003–2014, and for the year 2010, to detect the flood time, duration, and intensity. The cumulative precipitation in Punjab was studied for the five stations with three climatic divisions (southern, central, and northern), for the period of 2002–2014, using the daily precipitation data at specific intervals (P_i), ranging from 16 days to 1 year (D-16 to D-384), to investigate the region dynamically. Hence, the daily precipitation is measured in mm for the validation of the VTCI time series values over the five weather stations of Punjab.

2.3. Methods

We considered the MODIS data that captured the phenological development and variability of a crop at each pixel, having a high proportion of the crop of interest due to the high temporal resolution of the data [46]. Next generation trends in data development for global research and their manifestations predict changes for the MODIS Terra (EOS AM) and Aqua (EOS PM) Earth science (<https://modis-land.gsfc.nasa.gov/>, accessed on 22 December 2022). The daily data are produced at a 1 km spatial resolution on the geographically aggregated LST, over 8-day intervals, whereas the NDVI (the ratio of red and near-infrared reflectance) products span 16-day intervals for the 12-year period, using MODIS Aqua data products. This provides continuity for the time series applications in this study [47,48]. Several authors have suggested using a trapezoidal plot of the LST and NDVI to

portray the therapeutic quantitative parameters of drought and soil moisture [48–50]. Furthermore, a negative association between the LST-NDVI and crop moisture index is visible when the three variables are plotted against one another [48]. In addition, the GFMS model was evaluated in terms of its performance and accuracy for flood detection against flood events, utilizing the real-time integrated satellite TRMM and TMPA data products that were obtained from the NASA Goddard TRMM/GPM Precipitation Processing System (PPS) [50].

Our strategy utilizes the maximum–minimum value compositing (MVC) technique to produce the 16-day maximum-quantity composite LST data, with a 16-day factorial gap to identify the drought and LST_{\max} , and LST_{\min} in a triangle space of the LST vs. NDVI. To understand the importance of the solar zenith angle, it was transformed into a composite of the LST and NDVI at their greatest value throughout several years [48]. The MVC technique reduces the effects of the solar zenith angle, the satellite’s view angle, and the orbit drifts and cloud contamination [51]. MVC was proposed by Wan et al. [52] and Sun et al. [53], and their concerns were conclusively put to rest by the consistent use of the maximum-value annual and multi-year composites of the LST and NDVI products.

The edges can be calculated in one of three ways: (1) the maximum values from each year are used to composite the LST and NDVI products during the specified time frame; (2) by using the maximum values from multiple years’ worth of data during the specified time frame; and (3) by using the maximum values from multiple years’ worth of data during the specified time frame to calculate the warm edge, and the maximum and minimum values from multiple years’ worth of data to calculate the cold edge, as shown in Figure 2a. The VTCI plots, which are located in the LST-NDVI space, are optimal for identifying the warm–cold margins, drought, and flood conditions [52,53].

During the VTCI time series, the thermal content of the soil and vegetation, as well as the LST_{\max} and LST_{\min} , are contained within the triangular/trapezoidal region, which is known as the LST-NDVI feature space (see Figure 2a) [52–54].

$$VTCI = \frac{LST_{NDVI_i \cdot \max} - LST_{NDVI_i}}{LST_{NDVI_i \cdot \max} - LST_{NDVI_i \cdot \min}}, \quad (1)$$

where

$$LST_{NDVI_i \cdot \max} = a + bNDVI_i, \quad (2)$$

$$LST_{NDVI_i \cdot \min} = a' + b'NDVI_i. \quad (3)$$

Hence, $LST_{NDVI_{i \cdot \max}}$ and $LST_{NDVI_{i \cdot \min}}$ show the max and min. The LSTs of the pixels with the same $NDVI_i$ in the region are considered for the study. a , b , a' , and b' can be estimated from a larger area, where the soil moisture spans from the wilting point to the field capacity at the pixel level on the surface. The coefficients can be estimated from the scattered plots of LST and NDVI, and Equations (2) and (3) describe the tentative judgment indicators in the shape of scattered plots. Additionally, due to the extensive region expansion, the a , b , a' , and b' evaluate the predicted VTCI space plot of the LST dissension middle pixel with a strong and noticeable effect from the NDVI. This achieves regional and geographic pixel-level NDVI-LST space plots for the degree of soil wetness at the superficial horizon and sagging location. The remotely detected radiant fluxes are standardized by the wavelength and temperature in the VTCI drought-monitoring method. This provides a transition that uses the NDVI and LST. The VTCI drought monitoring yields different results at different time scales, and the scale of 16 days was selected, as it is more promising and practical [52–54].

In addition, the geospatial near-real-time coupling (NRTC) approach is used to retrieve this information alongside the multi-year data for daily precipitation, resulting in a more precise association (linear correlation coefficient) with the VTCI values. There is a

relationship between the accumulated precipitation data on the ground each day and the pixel-area VTCI values that were received over the same time period. There is a linear relationship between the VTCI and the regular cumulative precipitation values, between 2003 and 2014 for the VTCI, and between 2002 and 2014 for the precipitation data, with the range of this relationship being from 16 days to a year. Similarly, in the year 2010, the 1-year VTCI values were in a relationship with the daily cumulative precipitation in a certain period (P_i), from 16 days to 1 year during the 2009–2010 TPCP for the validation of the flood events detection.

$$VTCI = A_i TPCP_i \times B_i \tag{4}$$

In consideration with the accumulative precipitation data (TPCP) ranges (from 16 days or D-16 to 384 days or D-384) during 2002-2014 is the relationship within certain time periods P_i , which is based on the linear regression model. Similarly, for the determination of the drought and flood during 2010, the relationship is in consideration at D-009 to D-361, with the TPCP ranges (from 16 days or D-16 to 384 days or D-384) during 2009–2010 for the linear correlation coefficient within certain time periods P_i being based on the model of linear regression (see Equation (5)). The assessment of the VTCI drought, flood, and WAC edges utilized the NDVI and composited LST data, based on the MVC method, and for the validation of the drought and flood, we incorporated the TPCP in certain P_i using a regression equation method, as shown in Figure 2b. Hence, it is intended to validate the drought and flood using the NRTC approach, in order to employ the daily meteorological ground-measured precipitation data and its departure from normal monthly precipitation, with VTCI values from five stations for the plain of Punjab, Pakistan. The NRTC approach is used to correlate each weather station’s VTCI values with the accumulative precipitation data for the validations during the 12-year time series. Hence, the defined TRMM/TMPA anomaly is considered for the one-year (2010) flood in a retrospective manner against the region and its five weather stations’ runoff stream flow, stream flow, and flood detection/intensity observations of the flood events from north to south, over the plain of Punjab, Pakistan.

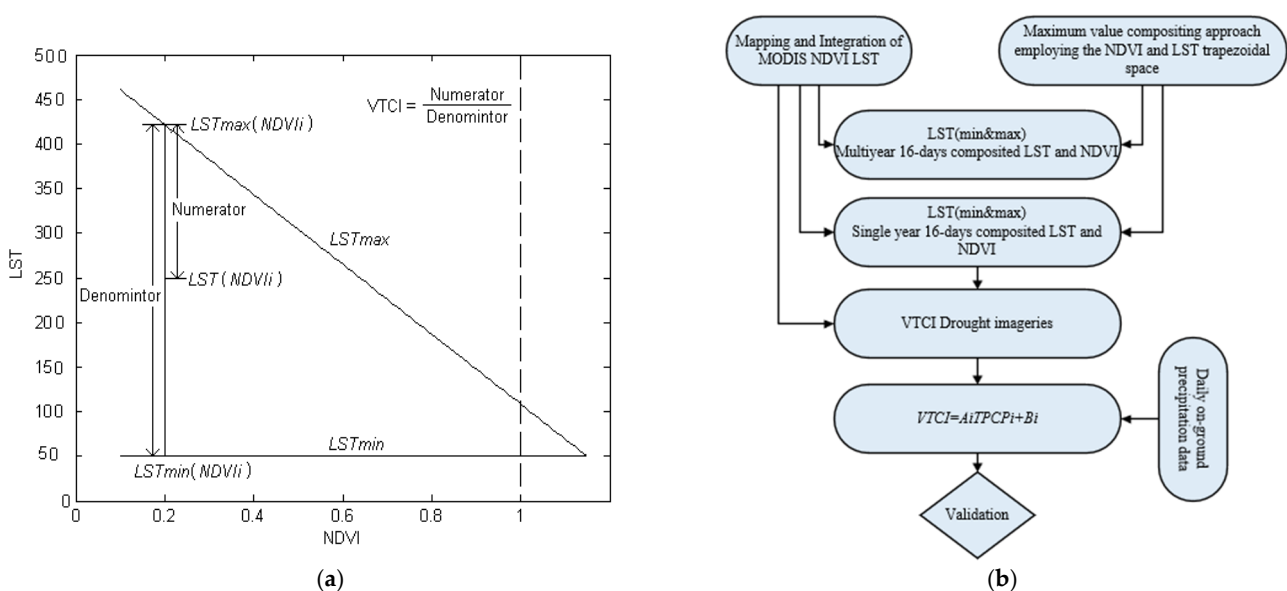


Figure 2. Schematic diagram of VTCI using the MVC method for drought, flood, and warm and cold edges, which are based on the linear regression equation. Where (a) presents the MODIS data from processing to validation using the VTCI approach, and (b) shows the trapezoid MVC method incorporating the single-year and multiyear acquired data products’ composite LST and NDVI data, which yields the edges and drought imageries with a 16-day difference.

To validate the drought and flood conditions in near-real-time, we utilized the geospatial NRTC method for the VTCI values and precipitation data, retrieving the pixel area values of the VTCI imagery at (1 km) and establishing a correlation with the TPCP data (the input data should be a vector of the precipitation values) across multiple stations.

3. Results and Discussion

3.1. Determining Drought, 'Warm and Cold Edges' and Flood

Since the detection of drought and flood, the SPI was proposed for a long period, extended from several months to years. Due to certain limitations in drought and flood determination for a short period (e.g., days or weeks), Zeng and Lu [55] objectively determined monsoon onset and retreat dates from seasonal cycles of perceptible water with certain criteria, whereas Lu E [55] determined the start and end dates (the duration and strength) of the flood and drought from the seasonal cycles of WAC. In this research, the VTCI method represents the sensations of heat that cause arduous effort and establish separation for the WAC edges, and the identification of the drought and flood occurrences (time, duration, and strength) across the target region. The soil moisture (wetness) is a reflection of the agricultural and hydrological influences over the region, and VTCI uses remote-sensing data (i.e., the integration of LST and NDVI) to measure drought levels. In addition, the VTCI is favorable for indefinite periods/seasons in monitoring the drought, as well as determining and validating the flood and the identification of the WAC edges over the region.

Utilizing the maximum values for each year, as well as the cumulative maximum values for the WAC edges over a specific time period, can help to determine the VTCI drought. The maximum–minimum-value-compositing approach was used for the detection of cold edges during the period from D-009 to D-169, spanning 2003–2014. Figure 3 illustrates how this approach was used to create composite LST and NDVI data, using multiyear maximum values to determine the warm edges and multiyear maximum–minimum-value composite LST products to detect the cold edges (3a, b). We found a strong correlation between the NDVI and LST for D-073 (2003–2014) of about 0.89, followed by 2003, 2010, 2011, and 2014, at the rates of 0.76, 0.72, 0.67, and 0.58, respectively. Figure 3c–f, on the other hand, shows the years 2003, 2010, 2011, and 2014, at D-073, utilizing each year's maximum-value composite LST and NDVI products for the given time period. Equations (5) and (6) illustrate how the WAC edges at D-073 are determined for single-year and multiyear data with specific periods (6). Equations (7) and (8) illustrate the flood events in terms of the soil moisture levels at the time of 2010, and also exhibit the determination of the WAC edges at D-217. This shows the variation in and at D-073 during the 2003–2014 multiyear and single-year maximum–minimum techniques during 2003, 2010, 2011, and 2014, respectively. Similarly, at D-217, during the flood events of 2010, the single-year maximum–minimum techniques were used to determine the WAC edges. Hence, the VTCI imageries' values are presented in Tables 1 and 2 for the drought during 2003–2014 and the drought and flood during 2010, in particular. The WAC edges for the multi-year and single-year are presented for specific days of the year:

$$LST_{NDVI_i, \max} = 335 - 25 \times NDVI_i \quad (5)$$

$$LST_{NDVI_i, \min} = 294 + 0 \times NDVI_i \quad (6)$$

$$LST_{NDVI_i, \max} = 330 - 25 \times NDVI_i \quad (7)$$

$$LST_{NDVI_i, \min} = 285 + 0 \times NDVI_i \quad (8)$$

We used the same MVC method techniques for D-009 to D-169 during 2003–2014, using multiyear and single-year maximum–minimum techniques to determine the VTCI imageries and edges during the crop season of the winter wheat. In addition, for D-009 to

D-361 in the time of 2010, the single-year maximum–minimum technique was used to determine the WAC edges, as well as the VTCI imageries for the drought and flood detection (all seasons). In general, multiyear and single-year are utilized in terms of the WAC edges for further analysis for D-009 to D-169 during 2003–2014, and D-009 to D-361 for the year 2010, respectively.

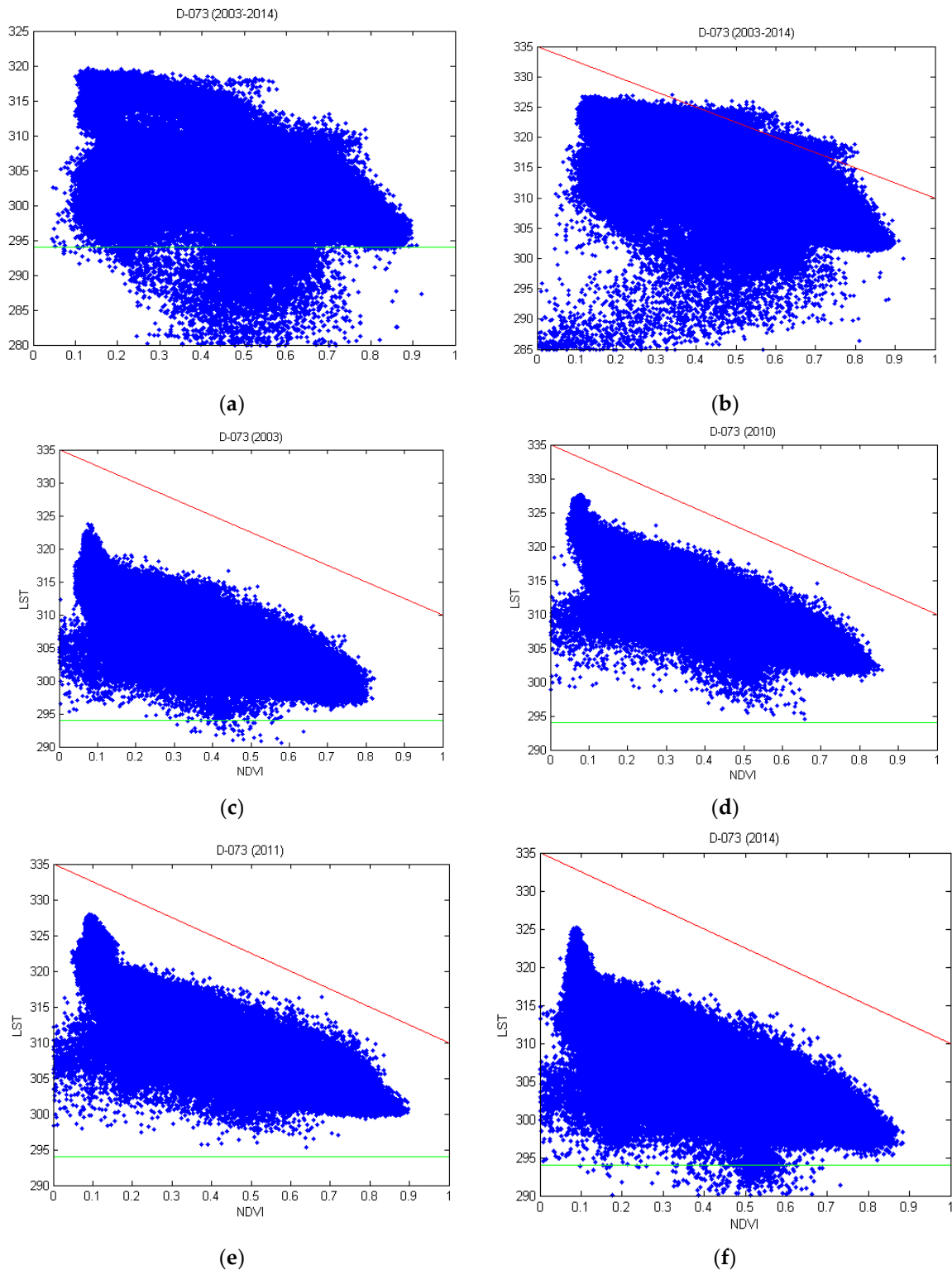


Figure 3. Plots of LST-NDVI in the first 16 days of March (D-073), spanning 2003–2014 for (a) the determination of the cold edge using the multiyear maximum-value NDVI products and maximum–minimum-value composite LST products, (b) the determination of the warm edge, using the

multiyear maximum-value composite LST and NDVI products, and the determination of the warm and cold edges, using the single-year maximum-value composite LST and NDVI products at D-073 during the years (c) 2003, (d) 2010, (e) 2011, and (f) 2014, plotting the single-year maximum-value composite LST and NDVI products in the first 16 days of March for the certain periods to determine the multiyear (2003–2014) and single-year (2003, 2010, 2011, and 2014) warm and cold edges, respectively.

The determination of the VTCI drought of each 16-day composite LST and NDVI data processing has been utilized for drought monitoring. The results are shown in Figure 4 and reveal the drought conditions for twelve-year periods between 2003 and 2014 at D-073. In contrast to the VTCI imageries, the estimated VTCI values of each of the five meteorological stations at D-073 during 2003–2014, and D-009 to D-361 during 2010, are shown in Table 1 and Table 2, respectively. The drought and flood occurrences are determined by these values. Furthermore, Tables 1 and 2, as well as Figure 4, display the categorization of the VTCI drought from 0–1, based on the quantitative VTCI statistics, which shows the normality or wetness in the majority of the plain at each weather station, at D-073 between 2003 and 2014. Table 1 and Figure 4 demonstrate a consistent, big-picture view of the drought conditions over the plain in both dry and wet years, together with the drought severity rating and range for each indication of dryness. Table 2 shows that, in 2010, the VTCI values at D-009 to D-361 ranged from (0.28 to 1.0). The VTCI values at D-201 are 1 over the five weather stations, whereas, at D-217, over four stations, the values were presented as 1, except for station 2 during the year 2010 (see Table 2). This determined the VTCI values of the season and flood events (time, duration, and intensity) during 2010. The results support the findings of previous studies that have been conducted across China and the USA [52,53]. They found that the analysis of the VTCI at the 10-day intervals shows that the VTCI profiles are different for irrigated and rainfed conditions across China. In the USA, they found that the VTCI is not only closely related to recent rainfall events, but also related to past rainfall amounts, which indicates that the VTCI might be a better and a near-real-time drought-monitoring approach.

Table 1. VTCI values in each of five meteorological stations (St.) at D-073 during 2003–2014, per pixel area.

VTCI D-041	Weather Stations				
	St. 1	St. 2	St. 3	St. 4	St. 5
2003	0.634858	0.632244	0.653159	0.682353	0.605664
2004	0.509368	0.582135	0.603486	0.566449	0.561656
2005	0.706754	0.727669	0.814815	0.739869	0.800871
2006	0.660566	0.601743	0.71329	0.715033	0.709368
2007	0.639651	0.691068	0.690196	0.663181	0.732462
2008	0.550327	0.544227	0.637908	0.610022	0.594771
2009	0.534205	0.622222	0.771678	0.647495	0.692375
2010	0.442702	0.457952	0.586928	0.48976	0.577342
2011	0.498039	0.535512	0.654902	0.566013	0.628322
2012	0.616122	0.685839	0.70719	0.643137	0.699782
2013	0.433115	0.646187	0.678867	0.620479	0.715468
2014	0.5939	0.684532	0.71939	0.659695	0.730719

Drought categorization on a scale of 0 to 1 or dry to wet: normality or wetness (1 to 0.57); slight mild drought (0.57 to 0.44); moderate drought (0.44 to 0.38); and severe drought (0.38 to 0).

Additionally, the soil characterization affects how severe a drought is; a lower VTCI value indicates a more severe drought, as shown in (Tables 1 and 2), in which the drought

results were lighter; this shows normality and could not find moderate or severe drought over the entire region at D-073, spanning 2003–2014. Similarly, the drought values at D-009 to D-361 during 2010 were determined, and show results from 0.28 to 1.00 on the fractional scale of the VTCI drought over the region, as shown in Table 2.

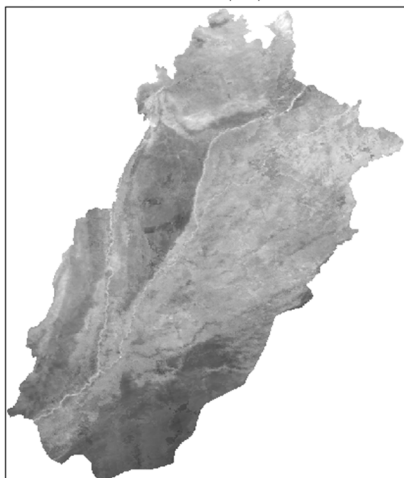
Table 2. VTCI values in each of five meteorological stations (St.) on the day of the year D-009 to D-361 during 2010, per pixel area.

VTCI–Day of the year 2010	Weather Stations				
	St. 1	St. 2	St. 3	St. 4	St. 5
D-009	0.70719	0.706318	0.807407	0.742484	0.776906
D-025	0.555556	0.549455	0.710675	0.653595	0.64793
D-041	0.55512	0.583878	0.658388	0.601307	0.660566
D-057	0.610893	0.537691	0.657952	0.648366	0.681046
D-073	0.442702	0.457952	0.586928	0.48976	0.577342
D-089	0.468845	0.542919	0.579085	0.495861	0.607843
D-105	0.382135	0.417429	0.396514	0.3939	0.432244
D-121	0.356427	0.479739	0.435294	0.367756	0.447059
D-137	0.282789	0.382135	0.308497	0.318954	0.330719
D-153	1	0.454902	0.494553	1	0.526797
D-169	0.412636	0.400871	0.45098	0.481481	0.454466
D-185	0.866231	1	1	0.611329	1
D-201	1	1	1	1	1
D-217	1	0.816558	1	1	1
D-233	0.284967	0.53159	0.547277	0.301961	0.586492
D-249	0.447495	0.547712	0.63573	0.478867	0.634858
D-265	0.367756	0.405664	0.499346	0.395643	0.514597
D-281	0.437473	0.541612	0.556863	0.471024	0.555991
D-297	0.31329	0.500218	0.385185	0.349891	0.483224
D-313	0.324619	0.504575	0.44183	0.4122	0.48976
D-329	0.3939	0.57342	0.362963	0.413943	0.42658
D-345	0.40915	0.512418	0.436166	0.412636	0.499782
D-361	0.375163	0.557734	0.430065	0.375599	0.473638

Drought categorization on a scale of 0 to 1 or dry to wet: normality or wetness (1 to 0.57); slight mild drought (0.57 to 0.44); moderate drought (0.44 to 0.38); and severe drought (0.38 to 0).

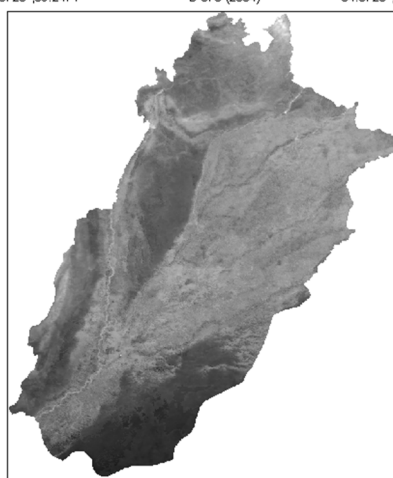
In the first sixteen days of March (D-073) during 2003–2014, drought was observed in the plain region, following favorable early winter wheat crop growing conditions, ahead of normality from the south to the north of the field. For D-073, over the entire period, considerable rainfall occurred across the selected region, thereby improving the growing conditions and allowing for the return to normal crop growing, due to sufficient precipitation. However, the well-established irrigation system over the region also plays a significant role in the vegetation conditions. To compare and contrast the two products, it is crucial to understand the 12-year VTCI drought at D-073 during the crop growing season, as shown in Figure 4, namely, the VTCI and TPCP (e.g., dry and wet conditions).

34.0725°;69.2471° D-073 (2003) 34.0725°;75.3907°



27.6917°;69.2471° 27.6917°;75.3907°

34.0725°;69.2471° D-073 (2004) 34.0725°;75.3907°



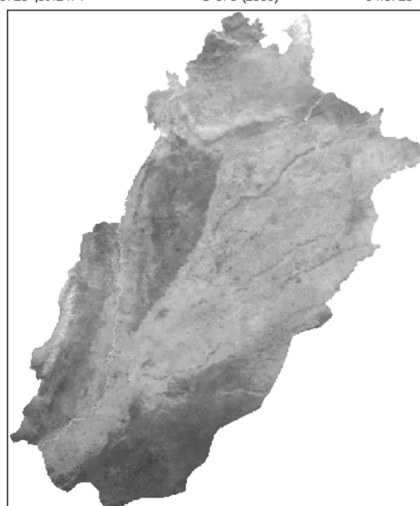
27.6917°;69.2471° 27.6917°;75.3907°

34.0725°;69.2471° D-073 (2005) 34.0725°;75.3907°



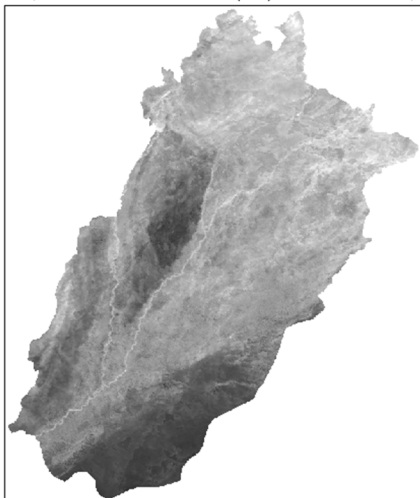
27.6917°;69.2471° 27.6917°;75.3907°

34.0725°;69.2471° D-073 (2006) 34.0725°;75.3907°



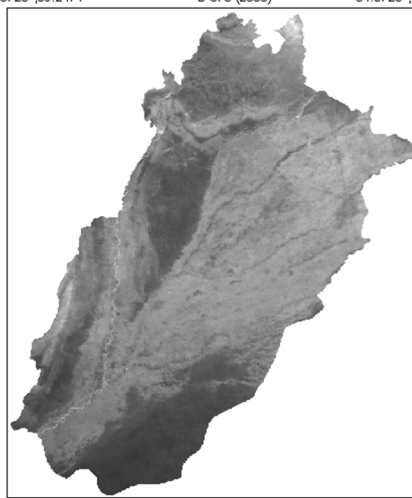
27.6917°;69.2471° 27.6917°;75.3907°

34.0725°;69.2471° D-073 (2007) 34.0725°;75.3907°



27.6917°;69.2471° 27.6917°;75.3907°

34.0725°;69.2471° D-073 (2008) 34.0725°;75.3907°



27.6917°;69.2471° 27.6917°;75.3907°

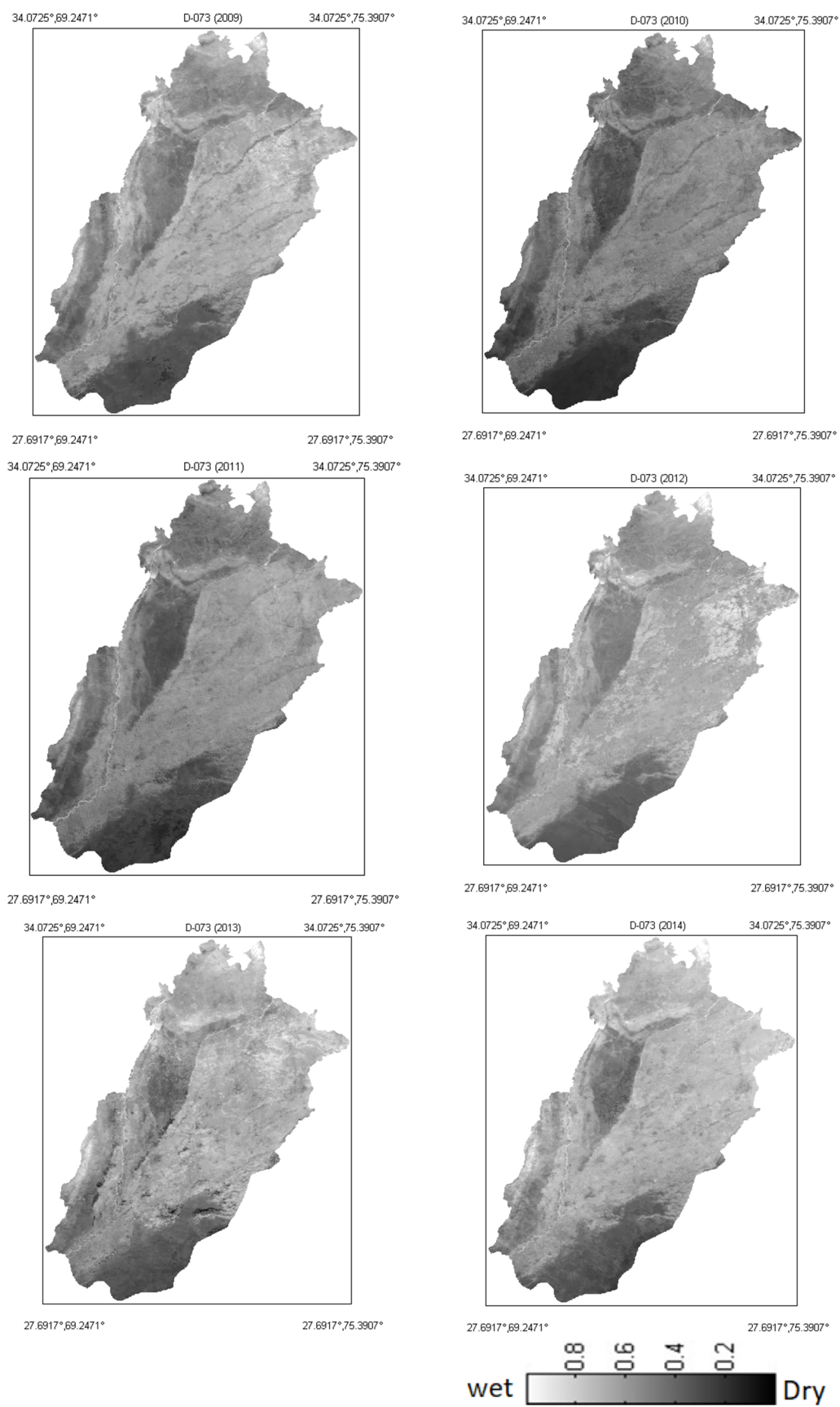


Figure 4. Determination of VTCI drought monitoring results on a scale of (dry to wet) or (0 to 1) in the first 16 days of March (D-073), using the single-year maximum-value composite of LST and

NDVI products to determine the warm edges and cold edges in 2003–2014, using the single year-maximum-value compositing approach to determine the warm edge, and the maximum–minimum-value compositing approach to determine the cold edges. This yields the MODIS VTCI drought imageries. The selected images are highly correlated during the winter wheat crop growing season at D-073 during 2003–2014.

The VTCI drought and flood categorization are based on a scale from 0–1 or dry–wet. The VCI values for the first sixteen days of March (D-073), spanning 2003–2014, are shown in Table 1, and the values for the first sixteen days of January to the last sixteen days of December during 2010 are shown in Table 2, respectively. This covers the VTCI values for the five stations (two stations over Multan, two stations over Faisalabad, and one station in Lahore, positioned alongside southern, central, and northern Punjab). These results indicated that the majority of the northern, central, and southern regions of the Punjab Plain areas do not experience more severe droughts during the winter wheat crop. The north-eastern and western Punjab Plain regions exhibit different precipitation patterns from the south, according to Adnan et al. [56]. Compared to the north and northeast, most of the farms in the south of the plain do not receive enough rainfall. This reveals that the rainfall deficit and lakes do not affect the crop condition. Additionally, during the twelve years (2003–2014), all the values were significant, indicating that most areas were normal during the crop growing season of the winter wheat, therefore, there is widespread agreement across the whole region that favors the optimum farming conditions for the 2003–2014 wheat farming.

3.2. Determining the Flood Using the GFMS Model

With the validation of the MODIS Aqua data products employing the VTCI approach and the results for the flood events during 2010, we considered the GFMS model, which incorporates the University of Washington variable infiltration capacity (VIC) land surface model, coupled with the University of Maryland Dominant River Tracing Routing (DRTR) model [57,58]. The VIC/DRTR coupled model is named the Dominant river tracing-Routing Integrated with VIC Environment (DRIVE) model. The GFMS model was evaluated in terms of its performance and accuracy for flood detection against flood events, utilizing the real-time TRMM rainfall-incorporated data product as the TRMM TMPA precipitation data product, which was obtained from the NASA Goddard TRMM/GPM PPS [59]. TRMM (NASA and the JAXA Agency joint mission) contributes a 17-year (November 1997 to April 2015) dataset of global precipitation and lightning for measuring rainfall events, flood, drought, and weather forecasting. The defined GFMS with the DRIVE model was considered for the one year (2010) in a retrospective manner against the five stations, in order to gauge the stream flow observations, as well as the flood events and cumulative precipitation from north to south, over the plain of Punjab, Pakistan.

The proposed GFMS model by Wu et al. [59], and the demonstrated results of the flood detection/intensity and flood stream flow from the five weather stations, incorporate the real-time quasi-global hydrological calculations at a 1/8th degree for the calculated water depth (mm) above the flood threshold, with temporal resolutions (3 hourly) at a relatively high spatial (~12 km) for the water stream flow. The flood detection/intensity and accumulative daily rainfall (~1 km) resolution is in good agreement with our results for the year 2010, which utilized the MODIS VTCI 16-day acquired imageries and daily precipitation data geospatially at a (~1 km) resolution, for the flood detection over the region run, retrospectively, for the year 2010.

Hence, the five rivers of Punjab mainly flooded during the summer of 2010 (monsoon), due to heavy rainfall and the snow melt of the Himalaya Mountain Range in the north of Pakistan. The flash flood from the monsoon rains 2010, lasting at D-227 and at D-229, is presented in Figure 5, crashing down from the Himalayan Mountain Range (called

'The Third Pole' of the world) in the north of Pakistan, through the south of the plain to the Arabian sea.

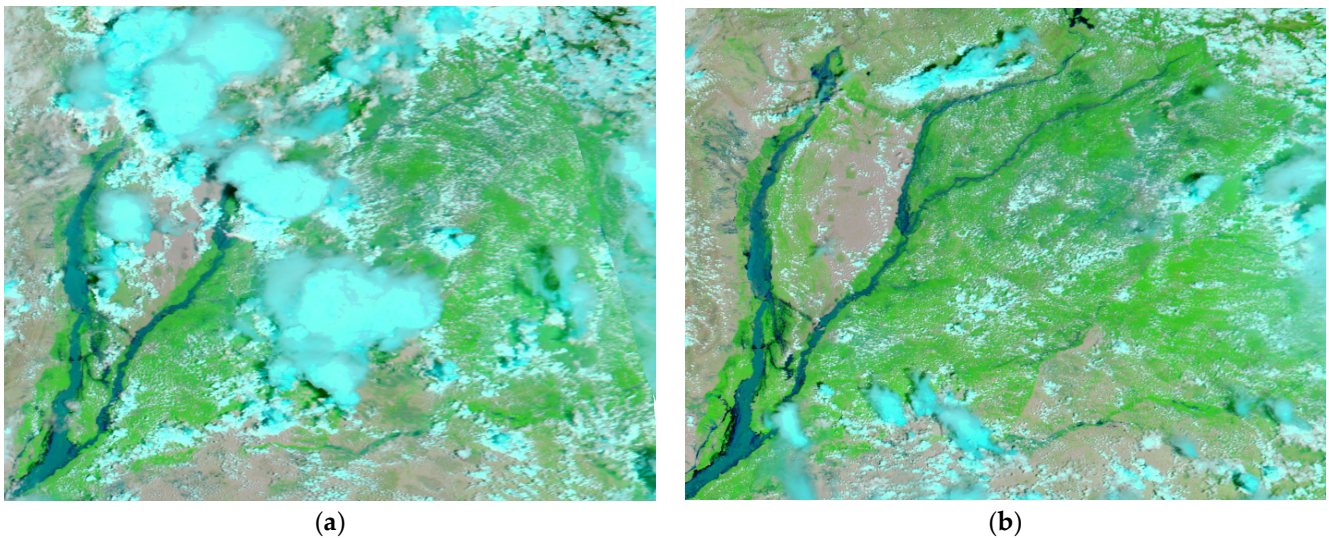
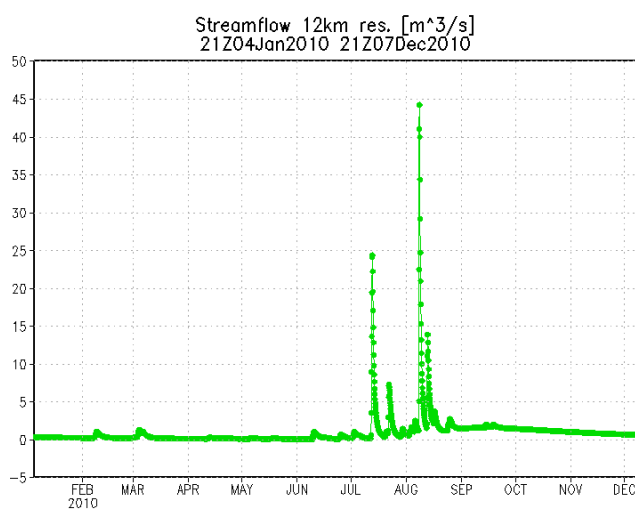
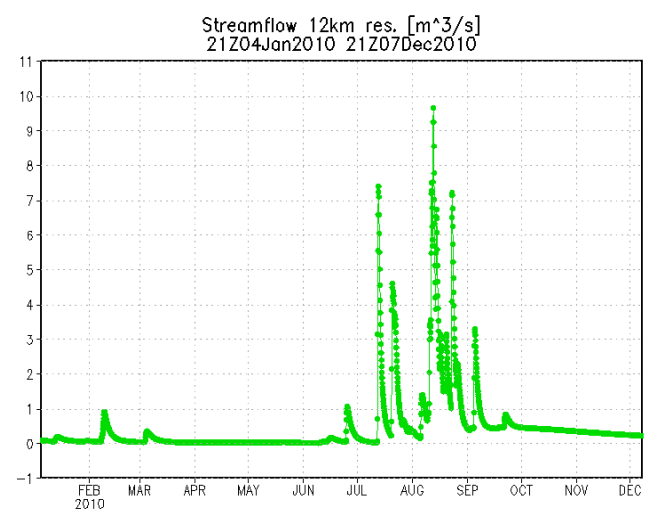


Figure 5. Flash flood from monsoon rains 2010 lasting (a) at D-227, and (b) at D-229, crashing down from the Himalayan Mountain Range (northern Pakistan), and muddy water swept over the south of the plain.

Muddy water swept over the south of the plain from the Indus Basin, across the five stations of the plain. Hence, flooding in the main Indus River of the plain passes through the northwest and lasts until the south of the plain (i.e., station 3 and station 5), which shows the flood stream flow at a 12 km resolution, as shown in Figure 6c,e, respectively. Hence, the stream flow events with temporal (3 h interval) and (~12 km) spatial resolution over the region (b to f) highlight the flood stream flow at a time series (21Z20July2010 to 21Z08Oct2010), which shows a maximum water flow above the threshold and ends in the south of the region, defining the plain to normal conditions, as well as the water flow in the Indus Basin, and also categorizing normal for the winter wheat crop seasons, as shown in Figure 6f.



(a)



(b)

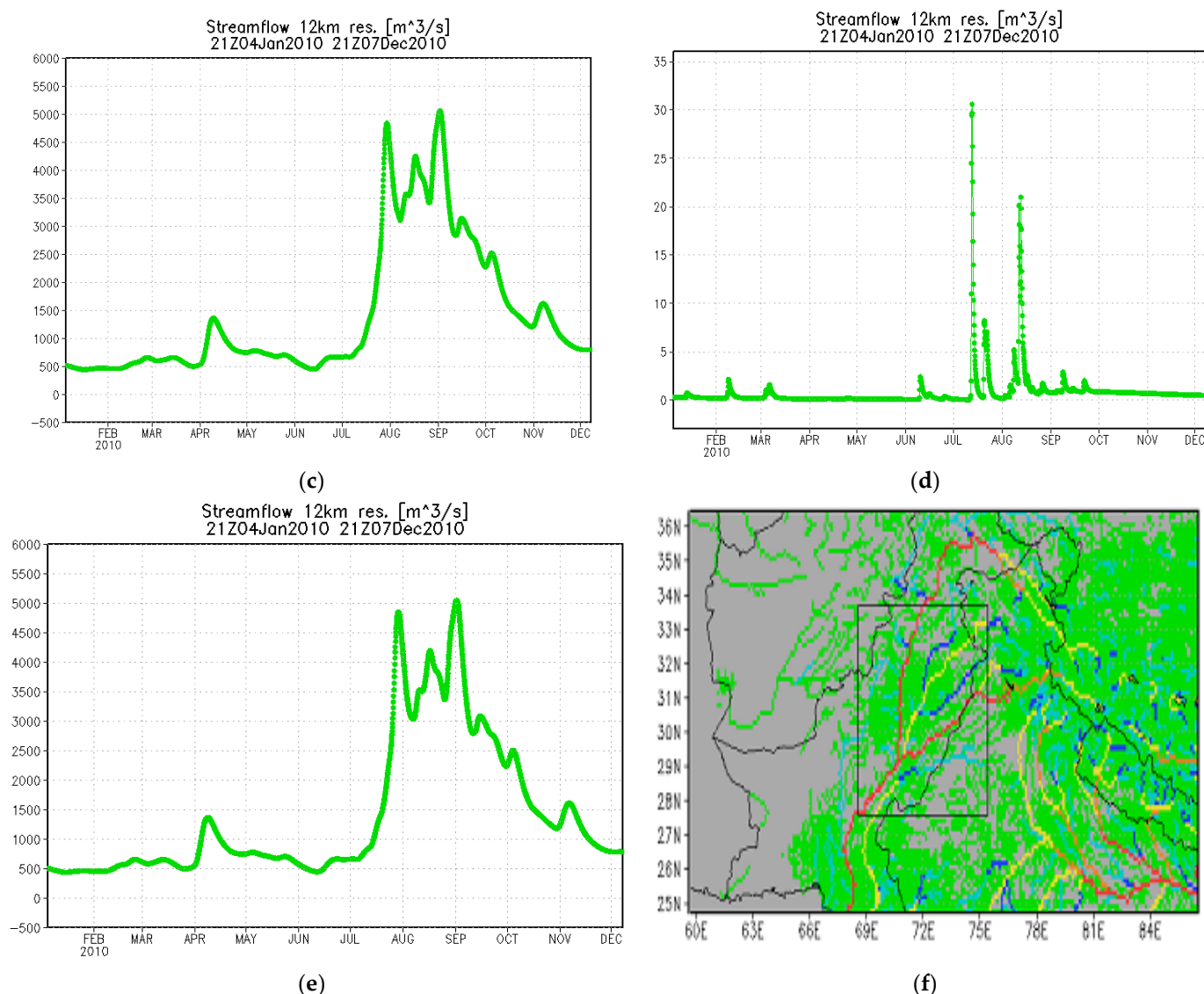


Figure 6. The captured stream flow events with temporal resolution (3 hourly) at relatively high spatial (~ 12 km) resolution over five weather stations (a–e) highlight the flood stream flow at time series (21Z04Jan2010 to 21Z07Dec2010), whereas, (a) represents St. 1, and (d) presents St. 4, showing the central area of the plain, while (b) presents St. 2 in the north of the plain, (c) represents St. 3, and (e) represents St. 5 in the south of the plain, respectively, which shows a maximum water flow above the threshold in the south of the region (the flood event happened in Punjab). (f) Indicates the maximum water flow in the Indus Basin.

Subsequently, Figure 7 shows the flood detection and intensity (the depth above the threshold) with a (~ 1 km) pixel area over the five stations, and reveals that the Indus River and four shallow rivers contribute in the form of wetlands, due to extreme moisture contents at D-201 and D-217 during 2010. Figure 7 demonstrates the flood intensity over the five stations, where (a) represents St. 1, and (d) presents St. 4, which shows the central area of the plain with a bit of flood intensity. Meanwhile, (b) presents St. 2 in the north of the plain, and shows the flood intensity but not severity. In addition, (c) represents St. 3, and (e) signifies St. 5, and shows the severe intensity of the flood events in the south of the plain, demonstrating the maximum flood intensity to be above the threshold in the south of the region, more so than in the north and central areas of the plain (i.e., St 1 and St. 4 are located in the south of the plain and face the stream flow of the water, passing through them to the Arabian sea, which is located in the south of Pakistan). Furthermore, (f) shows the overall flood detection/intensity to be above the flood threshold during

(21Z20July2010 to 21Z06Sep2010), with water depth in (mm) at a 1 km pixel area resolution, and presents the maximum flood intensity to be above the threshold of the conditions in the region. It has been well-documented in previous studies that these models can better forecast the category and extent of flood intensity, and can be applied to forecast flood in the plain [52], which further supports the findings of the study.

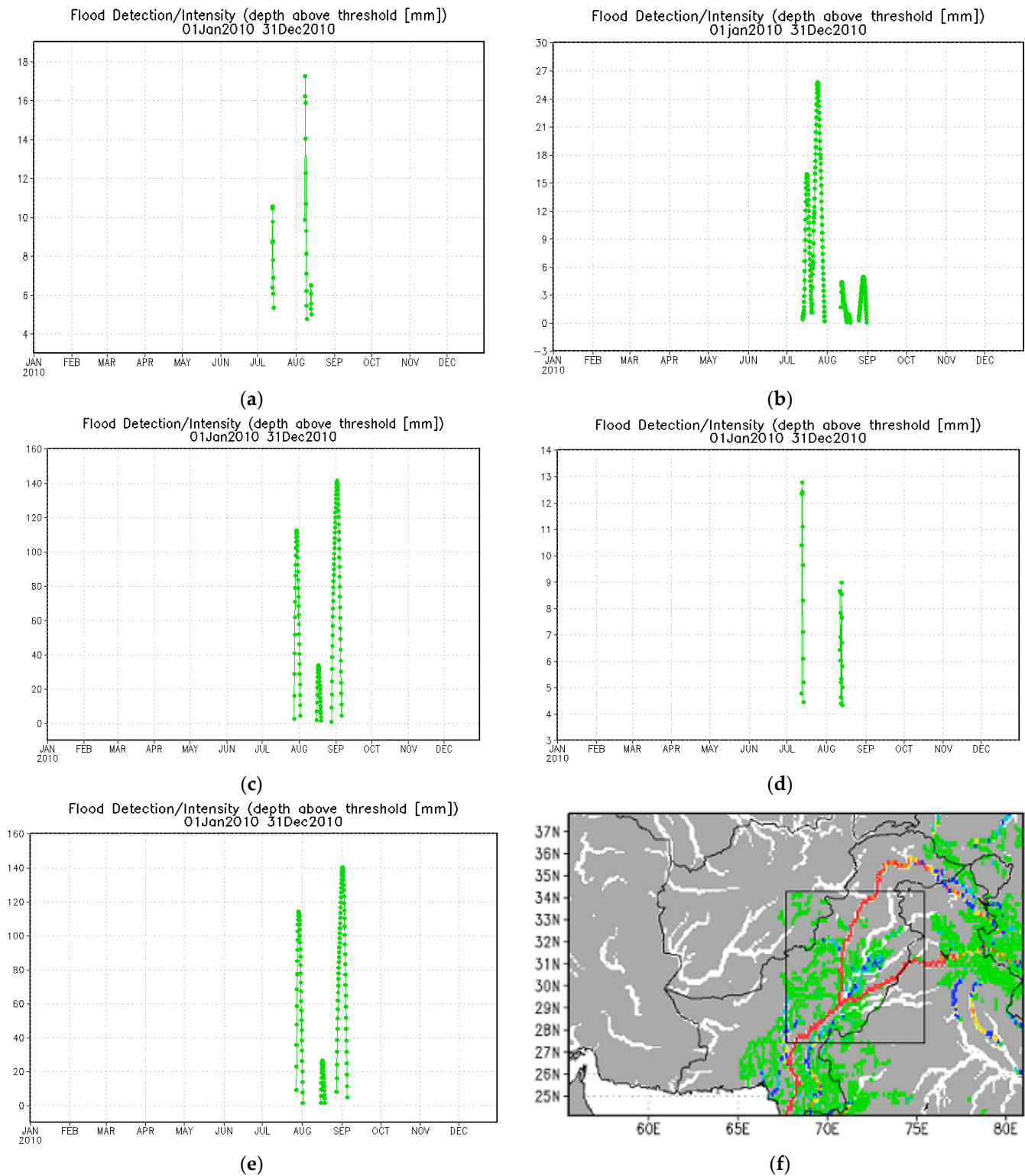


Figure 7. Flood detection and intensity above flood threshold at 3 h time intervals (01Jan2010 to 31Dec 2010), with water depth in (mm) with 1km pixel area over five stations, (a) represents St. 1, and (d) presents St. 4, showing the central area of the plain, while (b) presents St. 2 in the north of

the plain, (c) represents St. 3, and (e) represents St. 5, and shows the most intensity in south of the plain, which shows a maximum flood intensity above the threshold in the south of the region. (f) Shows the maximum flood intensity in the Indus Basin.

Figure 8 is in agreement with the PMD daily precipitation data, which are promising in validation with the VTCI imageries over the five weather stations (the relationship of the VTCI values and ground-measured daily precipitation data). The TRMM (1-day accumulative rainfall data) signifies our approach and data.

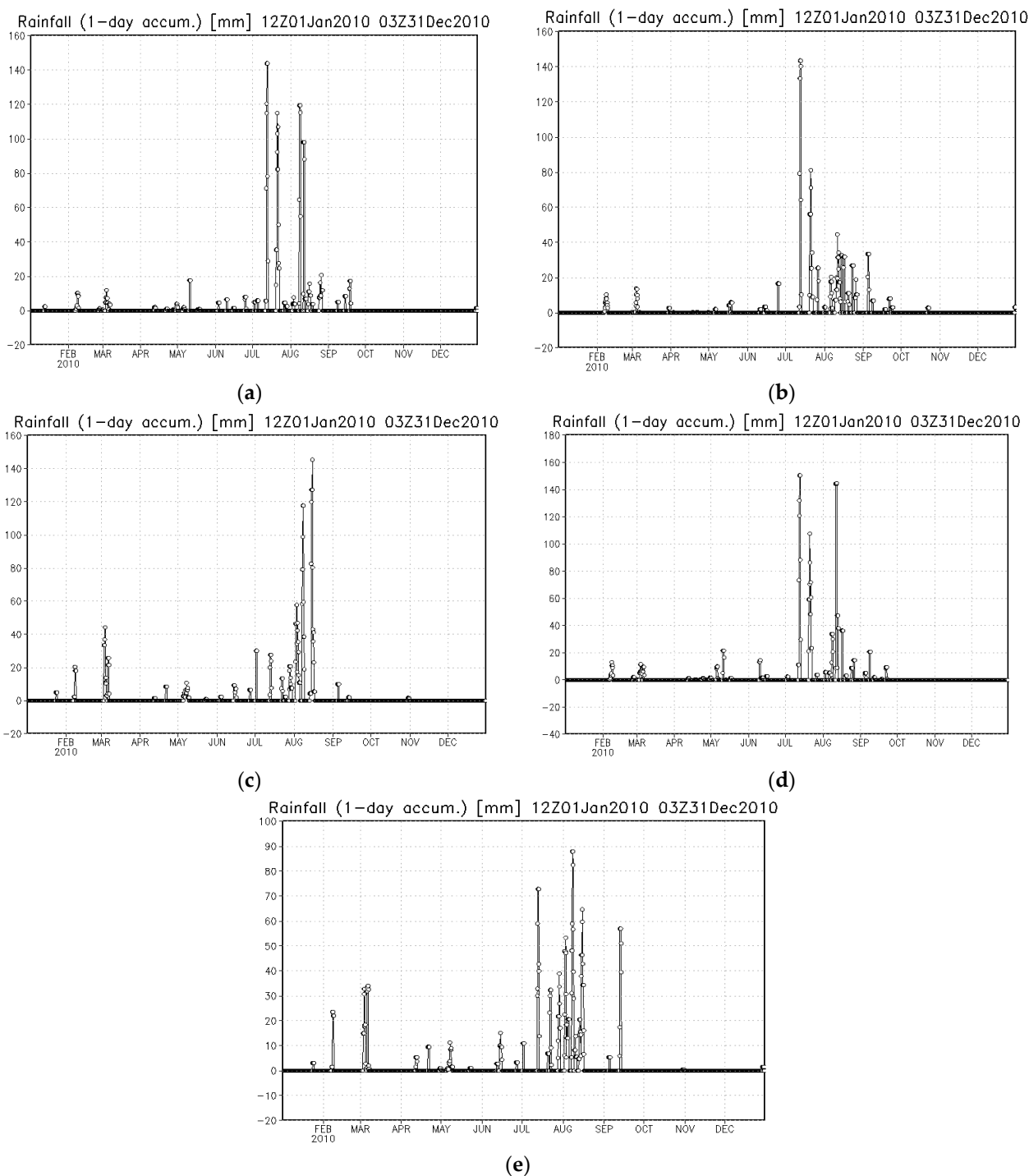


Figure 8. Real-time TRMM rainfall data events with temporal resolution (3 hourly) at relatively high spatial (~1 km) spatial-temporal evolution (real-time daily rainfall input data in mm), over five stations. Here, (a) represents St. 1, and (d) presents St. 4, showing the central plain, while (b) presents

St. 2 in the north of the plain, (c) represents St. 3, and (e) represents St. 5 in the south of the plain, respectively.

When determining the warm edges and cold edges across the Punjab Plain in 2010, the soil moisture levels at D-185, D-201, D-217, and D-233 were calculated using a single-year maximum-value aggregate of the LST and NDVI products (see Figure 9). This reveals the normal and flood events (time, duration, and intensity).

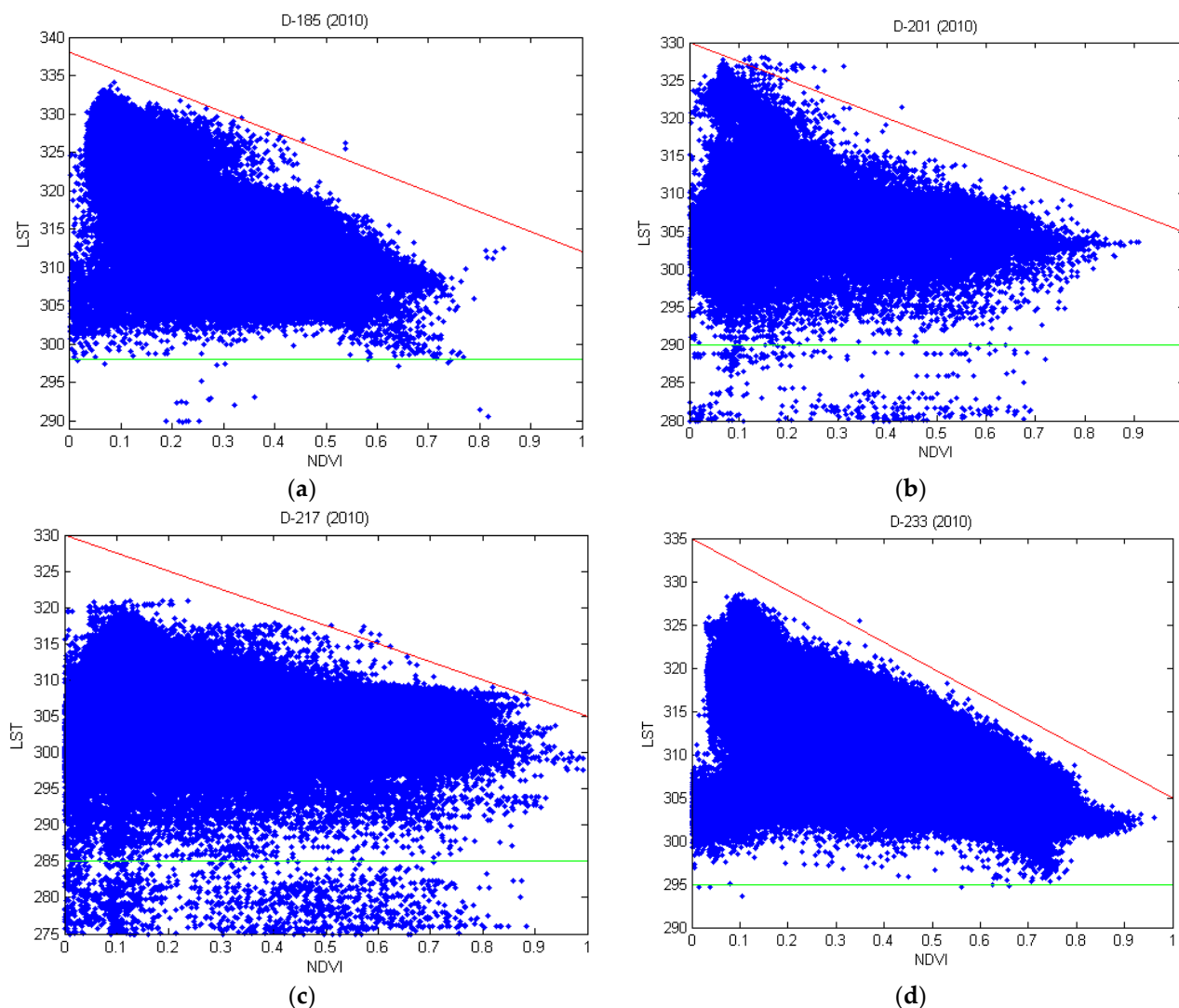


Figure 9. VTCI scatter plot of soil moisture contents in terms of warm and cold edges during 2010, with (a) at D-185, (b) at D-201 with heavy observed rainfall, (c) at D-217 demonstrating the flood events and extreme wetness, and (d) at D-233 showing the runoff of the water (normality) based on VTCI-approached scale categorization, dry to wet or (0.0 to 1.0).

In addition, the observed results of the GFMS model events in the inundation plot time series (00Z01Jan2010 to 21Z31Dec2010) at every five stations, for the flood detection/intensity at a 1 km resolution, and the flood stream flow at a 12 km resolution, as well as the accumulative precipitation plot at a 1 km resolution, are in considerably good agreement for the flood events. The GFMS model validates the flood detection/intensity at D-201 and D-217, and shows a very decisive and promising comparison with our results.

The use of the VTCI imageries and daily accumulative precipitation with collateral information was in line with a high accuracy for the determination of flood detection with the GFMS model, using real-time TMPA anomalies over the five weather stations in the region. Here, the 2010 flood reveals the flood time, duration, and strength, utilizing the

MODIS VTCI imageries, accompanied by the daily precipitation data, for validating the flood in the time series of 2010 over Punjab, which are in good agreement with the GFMS statistics. This shows that the GFMS model uses real-time TRMM precipitation data 3-step daily, and that local flooding statistics are in considerable agreement with the accuracy of the determination in the region [52]. In general, the determined flood detection and intensity, using the GFMS model that utilized the Goddard TRMM/GPM data products for the flood event detection with the flood event archives in the time series plots' results, validate our VTCI approach for the flood detection and intensity in 2010, and is very promising for our determined and validated MODIS VTCI results.

3.3. Validation of the Drought and Flood

The MODIS VTCI imageries examine the five stations situated at the southern, central, and northern demographic locations. We found that there was no slight mild drought, or moderate or severe drought conditions during the period from 2003–2014 at D-073as (Tables 1 and 3). At D-009 to D-361, during 2010, the drought is categorized with certain fractions, resulting in drought and wetness from 0.28 to 1.0 (i.e., severe drought to wetness) over the five weather stations (see Table 2). Tables 2 and 4 show the spatial variability of the flood (time, duration, and intensity) caused by the precipitation and flood. This generalizes the characteristics of the soil and land surface at D-201 and D-217 during the year 2010. The statistical results of the determined VTCI imageries were considered with the daily precipitation data that were collected from five stations, in order to validate the drought and flood, geospatially, over the area (see Table 4).

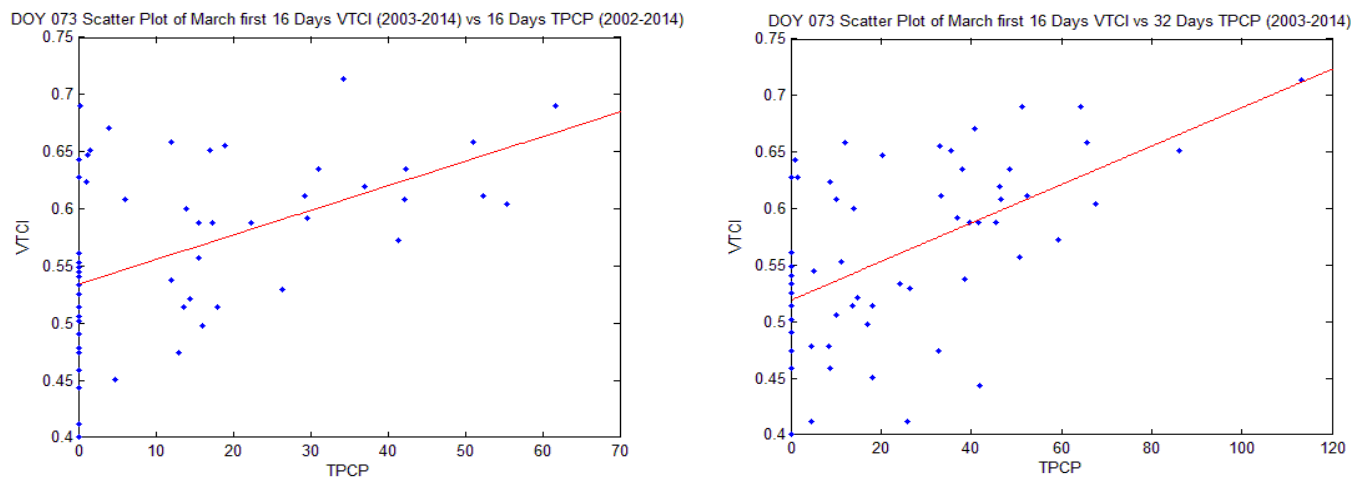
Table 3. Linear correlation coefficients between VTCI during 2010 and cumulative precipitation in the D-009 to D-361 during 2009–2010.

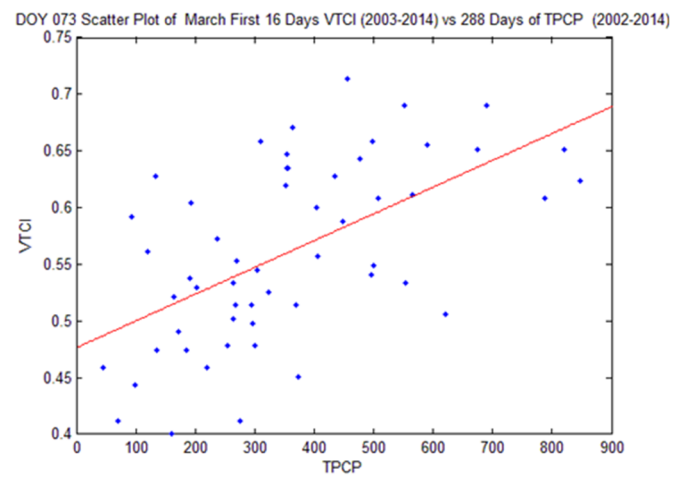
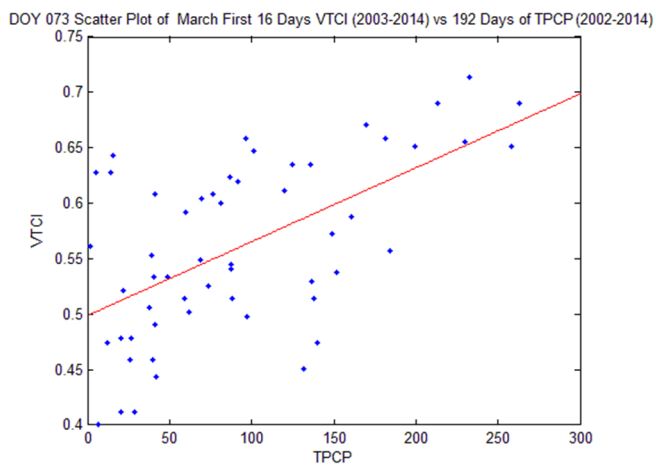
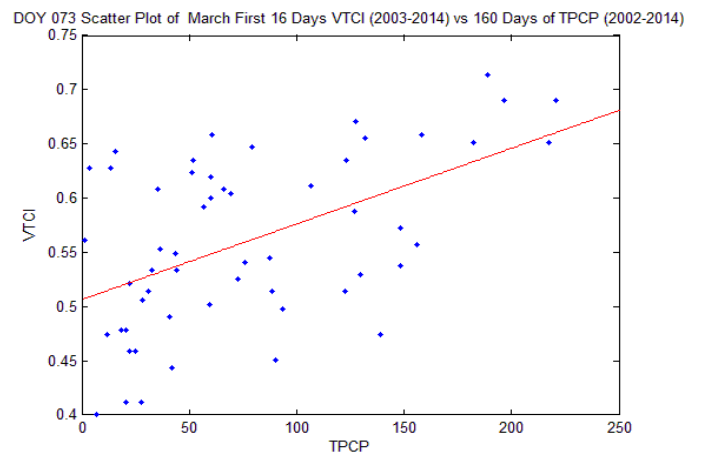
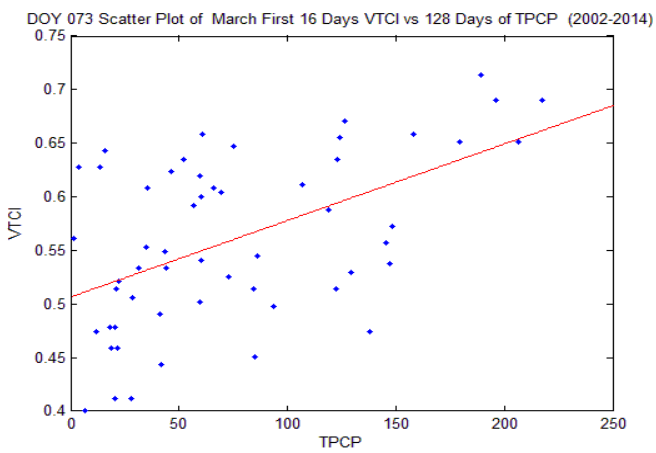
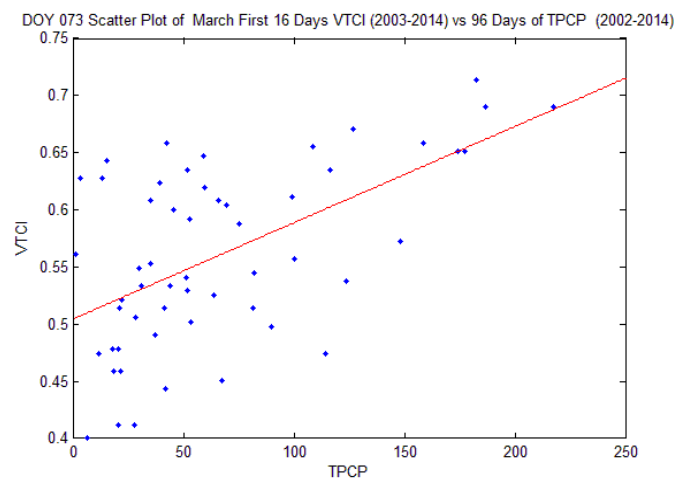
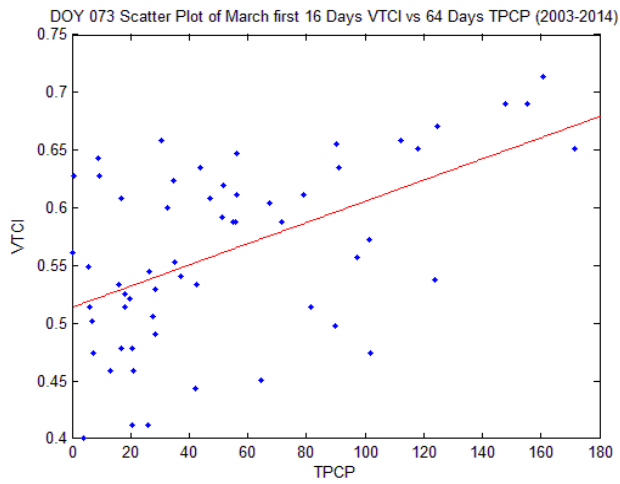
VTCI DOY	TPCP Periods								
	D-016	D-032	D-064	D-096	D-128	D-160	D-192	D-288	D-384
D-009	-0.2370	-0.2370	-0.2370	0.1902	0.7360	0.7494	0.9484	0.9426	0.9364
D-025	0.7707	0.6731	0.6731	0.7055	0.7160	0.3573	0.4164	0.5456	0.5881
D-041	0.5552	0.8509	0.8130	0.8130	0.7930	0.8174	0.8822	0.8706	0.8407
D-057	0.6663	0.6663	0.7374	0.73747	0.7292	0.7298	0.3822	-0.2044	-0.2223
D-073	-	-0.6777	-0.5691	-0.6163	-0.6163	-0.6083	-0.3467	0.9356	0.9562
D-089	-	-	-0.5707	-0.5058	-0.5058	-0.4871	-0.3691	0.8096	0.8024
D-105	0.0579	0.0579	-0.0395	0.0494	0.0759	0.0759	0.0544	0.2428	0.2017
D-121	0.6399	0.7453	0.74535	-0.5590	-0.3661	-0.3661	-0.3502	0.8882	0.9767
D-137	-0.3942	0.6505	0.6618	-0.2967	-0.0898	-0.0878	-0.0878	0.9864	0.7055
D-153	0.4068	0.3925	0.5992	0.5992	-0.1453	0.0662	0.0662	0.9440	0.5541
D-169	-0.2972	-0.3412	-0.3553	-0.2760	0.9380	0.8019	0.9748	0.6764	-0.1636
D-185	-0.2373	-0.2278	-0.2233	-0.2667	-0.2667	-0.4596	-0.4078	-0.3914	-0.2077
D-217	-0.9365	-0.5398	-0.5350	-0.5330	-0.5498	-0.5498	-0.6216	-0.6026	-0.5628
D-233	0.8031	0.8321	0.9555	0.9554	0.9555	0.9577	0.9554	0.9544	0.9046
D-249	0.3012	0.2084	0.3447	0.4074	0.4109	0.4282	0.4282	0.4531	0.4791
D-265	0.1182	0.5447	0.8226	0.7347	0.7442	0.7444	0.7460	0.7490	0.7525
D-281	0.3447	0.7210	0.8607	0.9637	0.9723	0.9743	0.9770	0.9766	0.9741
D-297	-0.4590	-0.1984	0.6688	0.8888	0.8922	0.8973	0.8979	0.9000	0.8994
D-313	-	-0.4774	0.7258	0.8912	0.8997	0.8910	0.8953	0.8921	0.8920
D-329	-	-	0.40815	0.54791	0.5629	0.7039	0.7076	0.7027	0.7024
D-345	-	-	-0.2688	0.7983	0.9026	0.8481	0.8255	0.8347	0.8356
D-361	0.0569	0.0569	0.0569	0.0459	0.6350	0.8031	0.7483	0.7382	0.7346

VTCI values at D-201 during 2010 do not correlate with TPCP, whereas at D-185 and D-217, a negative correlation was established, which shows flood time, duration, and severity.

As shown in Tables 3 and 4, as well as in Figure 10, we also noticed that the VTCI imageries had a very strong association with the TPCP. A substantial association between the cumulative precipitation and VTCI values was found, according to statistical analysis, during the winter wheat crop's green-up stage. The strongest linear correlation between the TPCP at D-384 and D-073 ($r = 0.60$, $p = 0.005$) was found there (i.e., the relationship of the VTCI drought at D-073 or March's initial 16 days throughout 2003–2014, using D-384 or a year's worth of precipitation during 2002–2014). Notably, the results suggested that the VTCI is lower for drought and higher for wet conditions, which is in line with the findings of a previous study conducted in the USA [52]. At D-233 and D-281 during 2010, a significant correlation was noted that showed the normal condition. Additionally, at D-201, a nonlinear result was established, and at D-217, a negative correlation took place during the year 2010, which indicated the time, duration, and intensity of the flood. It was also noticed that there was a positive correlation taking place in early summer at D-169 (June's first sixteen days) between the VTCI drought from 2003–2014 with the TPCP spanning 2002–2014.

These intervals depict the green-up phases at D-073 (first sixteen days of March) of the VTCI values in substantial association with D-384 of the precipitation, as shown in Table 3 and Figure 10. We also examine the VTCI D-169 (June's first sixteen days) spanning 2003–2014 and the TPCP spanning 2002–2014, which show the drought normality in early summer. This shows that the VTCI drought and the cumulative precipitation anomalies had a noteworthy correlation. This demonstrates that the VTCI values are based on the periods (Pi) of the TPCP values (i.e., based on the past precipitation) (see Tables 3–4 and also Figure 10). The VTCI is based on both the previous precipitation and recent precipitation, in addition to the former. Since the Punjabi Plain is both rain-fed and irrigated, the farms in the northeast are heavily rain-fed. Compared to the north, the majority of farms in the south do not receive enough rainfall. The VTCI values are particularly promising for spotting irregularities in daily precipitation, according to the combination of the VTCI drought and regional cumulative daily precipitation data. The drought in Pakistan is especially concerning given the summer monsoon. The precipitation erraticism in Pakistan is due to an abrupt discrepancy in the circulation patterns of its weather systems, such as the western weather system and summer monsoon [20]. Pakistan receives 50% to 60% precipitation from the summer monsoon, while about 30% of its winter rainfall from the western system [6]. According to Table 3, the linear correlation coefficient for the twelve years at D-073 between the VTCI and cumulative precipitation was 0.60, which is significant. These results also show that the south and central regions have low-precipitation-termed low VTCI values, and that the northeast region has enough precipitation-termed high VTCI values (see Tables 3–4 and Figure 10).





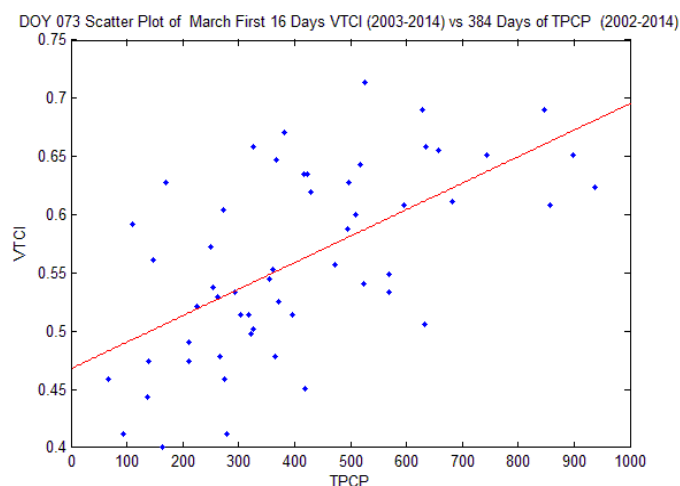


Figure 10. Linear Correlation of VTCI (D-073) and TPCP (D-016 to D-384) plots at five different meteorological stations for sixteen days to one-year, spanning over 2003–2014 for VTCI, and 2002–2014 for TPCP, in the given periods.

Furthermore, the VTCI imageries were investigated at D-009 to 361 throughout 2010, coupled with the daily precipitation anomalies spanning (2009–2010). It is observed that the linear correlation at D-073 was the strongest at the VTCI D-073 with TPCP D-384 during 2010, with D-384 or a twelve-month duration of the overall precipitation from 2009–2010, spanning over the entire period of the winter wheat crop season (see Table 4). Similarly, at D-233 and D-281 during 2010, a significant correlation was noted in the normal condition ($r = 0.95$ at D-233 and 0.97 at D-281 during the fall of 2010), which shows the normal condition as shown in Table 3. Moreover, regarding the flood time, duration, and intensity during the flood (21st July 2010), the correlation was negative at D-217, whereas D-201 was termed as nonlinear due to the soil wetness, which was categorized as '1' on the fractional scale by the determination of the VTCI imageries, as shown in Table 2 (water levels gradually increase due to heavy rainfall, which is termed as soil moisture and categorized as 1 or wet). This shows that the plain is irrigated, as well as rain-fed, and also that the impact of heavy rainfall causes unprecedented damage to the crops in the land of Punjab.

During the 2010 flood at D-201, there was a nonlinear presentation, and at D-217, a negative relationship was noted, which shows the flood time, duration, and intensity. These results are in line with the above statistical results of the cumulative anomaly precipitation and detect the VTCI drought and flood accurately over the selected time period, and with the GFMS model results, as shown in Figures 5–9.

In addition, considering the DPNP during a specific period established the VTCI value at D-073 spanning 2003–2014, for the sixteen days with a relationship ($r = 0.68$), and also noted a significant relationship of the VTCI values at D-057 and D-089, with the TPCP periods P_i at D-192 and D-160, respectively, as shown in Table 4. This reveals that the VTCI is not only closely related to recent rainfall events, but also to past rainfall quantities, indicating that VTCI is a better monitoring strategy in rain-fed and irrigated conditions.

Table 4. Linear correlation coefficient between cumulative anomaly precipitation (departure from normal monthly precipitation, DPNP) and VTCI, for the first sixteen days of January (D-009) to the first sixteen days of June (D-169), for the twelve years 2003–2014, with cumulative precipitation TPCP at certain periods Pi, from sixteen days (D-016) to one year (D-384) during 2002–2014.

VTCI DOY	TPCP Periods									
	D-016	D-032	D-064	D-096	D-128	D-160	D-192	D-288	D-384	
D-009	0.0117	0.0620	0.46525	0.6291	0.1570	0.3222	0.2914	−0.1466	−0.0968	
D-025	−0.7999	0.1592	0.2052	0.3612	−0.2640	−0.5359	−0.0127	0.2805	−0.0384	
D-041	0.3387	0.3280	0.2710	−0.1018	−0.3738	−0.5472	−0.4862	−0.5438	−0.5063	
D-057	−0.9345	−0.89083	−0.3413	0.05605	−0.6093	−0.5478	0.9779	0.7122	0.5646	
D-073	0.6843	0.1965	0.2488	0.3273	0.3854	0.2760	0.2999	0.4173	0.3281	
D-089	−0.8006	−0.7460	−0.4035	0.0513	0.9161	0.9168	−0.4185	0.7692	0.9036	
D-105	−0.1434	−0.0264	−0.0323	−0.02383	0.1392	0.7174	0.71658	0.5677	0.4826	
D-121	−0.60425	−0.5687	0.13461	−0.0141	0.5868	0.0112	0.24572	0.3922	0.4467	
D-137	0.17480	0.2468	0.30071	0.76973	0.5392	−0.3438	−0.5654	−0.5222	−0.4579	
D-153	−0.9582	−0.8856	−0.4946	0.29672	−0.8336	−0.5917	−0.6087	−0.5454	−0.6070	
D-169	−0.1996	−0.3497	−0.4601	−0.31107	0.8231	0.9686	0.6118	0.5814	0.5988	

We also looked into how time and season affect the link connecting the TPCP to the VTCI. It is favorable throughout the cooler season (winter), which runs from 2003 to 2014, and unfavorable during the 2010 flood and the year of record rainfall. The relationship between the VTCI for D-169 (June’s first sixteen days during 2003–2014) with the TPCP from the periods of D-016 to D-384 (sixteen days to one year during 2002–2014) has a positive correlation and was established from 0.47–0.60. In general, it was noted that, at D-169, there was a positive correlation that took place in early summer, which indicates that no severe drought was found during 2003–2014. This demonstrates that the VTCI and TPCP connect strongly in winter and late summer. In particular, the VTCI imagery offers a better map of all the areas for drought and flood over the plain of Punjab from D-009 to D-169 from 2003 to 2014, as well as from D-009 to D-361 from 2010 onward. The evaluation of the VTCI for the crop growing season demonstrated that it is the best drought approach during this season. It also accurately detected the winter drought conditions and is capable of providing a near-real-time indicator of the extent, intensity, onset, and duration of the vegetation condition, as well as of determining and validating the flood using the MODIS VTCI imageries. This study shows broad agreement, as the MODIS LST and NDVI imageries have been used to generate and validate the VTCI for the droughts, monitoring over the southern Great Plains of the United States. This is also in agreement with Sun et al. (2008), who have used the VTCI for drought monitoring in Guanzhong, China.

The spatial and temporal observations demonstrate the land surface drought conditions throughout the periods of 16 days to 12 months, where the accumulative precipitation had a significant correlation with the VTCI time series values, varying at five weather stations during 2003–2014. The relationship between the VTCI values and the total accumulative precipitation (TPCP) was very significant for the short time series in comparison with the long time series during the 12-year period. The weight correlation coefficients between the VTCI and the accumulative precipitation decrease with the increase in time series during 2003–2014. Based on our investigations of droughts, and the 2010 flood, which severely affected the region from D-201 to D-217 and D-233 to D-361 during 2010, the correlation was categorized as anomalous for the years 2011–2014, as well as for the twelve-year winter wheat crop season spanning from 2003–2014, in particular. The results of the early steps are in good agreement with those acquired by the VTCI imageries over the plain of Punjab, Pakistan, according to an examination of the vegetation and temperature-related drought indices. The five stations’ recorded precipitation data from the ground are taken into account with the geospatial NRTC approach, in order to validate and quantitatively monitor the area. This shows that the area witnessed heavy rainfall and its worst flood during 2010, and that it presented dry and wet spells with indistinct variations in the precipitation over the region in the 12-year period.

The results demonstrate that, in the crop field of Punjab, there is good agreement between the validation of the remote sensing data and the measured precipitation data that were used to classify the drought, flood, and WAC edges during the time series of the VTCI, under both rainfed and irrigated conditions. The investigation of the linear relationship between the VTCI and annual precipitation confirms that the VTCI is a superior and near-real-time method for monitoring drought and flood conditions, since it is so closely related to rainfall events, while also being based on precipitation history. This learning shows the significant capability of the MODIS VTCI imagery (the VTCI time series values) for dry and wet conditions (time, duration, and intensity) during the year 2010, using MODIS LST and NDVI data products. This reveals the dry/wet conditions and depends on the soil characterization: a lower value of the VTCI results in dryness severity, and higher values of the VTCI result in extreme wetness. Additionally, the employed GFMS model, using the TRMM and TMPA satellites' data products for the deluge plot time series (flood events and spells) over the region and the five weather stations with spatial and temporal observations, concludes that the stream flow events, with temporal and spatial resolutions over the region, highlight the flood stream flow at the time series (21Z20July2010 to 21Z08Oct2010), which shows a maximum water flow above the threshold and ends in the south of the region, presenting normality on 8 October 2010.

The present study will draw positive attention to young researchers who are working on flood and drought evolution, as well as policymakers working on sustainable solutions, providing broader evidence regarding the flood- and drought-stressed areas across South Asia. Moreover, in the future, this study will provide a new platform to enhance VTCI-based investigations into different aspects of South Asia. To advance the identifications and predictions of flood and drought, further detailed examinations are required, using remote sensing data from different sources and a diversity of flood and drought indices for the study area.

4. Conclusions

This study investigated the 1998–2002 severe drought and 2010 flood impacts for the target region, during the winter crop season for 12 years (2003–2014) and the whole year of 2010. This study is the first of its kind to investigate the flood and drought impacts on the winter wheat crop growing seasons using the VTCI index, across the Punjab province of Pakistan. In the present study, the twelve years of drought that were evaluated throughout the winter wheat crop growing seasons were subjected to wet conditions and a light drought was considered. The demonstrated investigation recognized the drought and the WAC edges, as well as the flood time, duration, and intensity. This suggests that the VTCI could detect the precipitation and moisture in agricultural land for the 12 years during 2003–2014, and during the year of 2010. It was also observed that the south and central parts of the plain had low-precipitation-termed low VTCI values, and that in the northeast, there were enough precipitation-termed high VTCI values. Between 2003 and 2014, the VTCI and TPCP had a positive and highly significant connection at D-073 ($r = 0.60$). This connection shows a strong link between the VTCI imageries at D-073 from 2003 to 2014 and the TPCP from 2002 to 2014. During the 12 years, there was a positive correlation between the VTCI and the cumulative precipitation (i.e., the relationship of the VTCI data products from (D-009 to D-169), except D-153, with the TPCP rainfall data for the periods (D-128, D-160, and D-288)). During the 2010 flood, in D-217, the correlation was shown as negative, while at D-201, it was established as nonlinear, whereas at D-233, there was a significant relationship. This shows that the 2010 flood (time, duration, and strength) is considered to have flood normality for the winter season. It is noteworthy that all the NDVI, LST, and VTCI values are appropriate for monitoring drought during the winter wheat crop's growing season, as well as for determining flood when considering NRTC for the validation of drought and flood. Since the southern, central, and northern parts of the region were in a normal drought between 2003 and 2014, the VTCI time series

values under the rain-fed and irrigated conditions were better in the south than in north-east. This also shows that there was no impact of the flood on the winter wheat crops during 2011–2014, and as a whole during the twelve years spanning 2003–2014.

In addition, the considered GFMS model for the evaluation of the inundation plot time series, at each of the five stations, was based on the temporal resolution (3 hourly) during the 2010 flood detection/intensity, at a relatively high spatial (~1 km) resolution and flood stream flow at a high spatial (~12 km) resolution, and the accumulative precipitation plot at (~1 km) resolution demonstrates the flood detection/intensity at D-201 and D-217, and shows a very decisive and promising result. Finally, the VTCI achieves high robustness and accuracy, which indicates that the proposed index is the best indicator of the VTCI imageries over the region. This study demonstrates the VTCI's excellent sensitivity to the rainfall and soil moisture levels on farmland.

Our findings indicate that the VTCI can be used as a superior indicator for drought monitoring and flood detection in rain-fed and irrigated areas throughout the year. In support of the VTCI approach, the employed GFMS model, using the TRMM and TMPA satellites' data products for the deluge plot time series (flood events and spells) over the region and the five weather stations with spatial and temporal observations, concludes that the stream flow events, with temporal and spatial resolutions over the region, highlight the flood stream flow at the time series (21Z20July2010 to 21Z08Oct2010), which shows a maximum water flow above the threshold and ends in the south of the region, presenting normality on 8 October 2010. The flood detection/intensity above the flood threshold during (21Z20July2010 to 21Z06Sep2010), with water depth in (mm) at a 1 km pixel area resolution and maximum flood intensity above the threshold, presents normality on 8 October 2010, and demonstrates the time, duration, and intensity of flood and the heavy rainfall in the region. This exhibits that the flood stream flow, detection, and intensity are very decisive and promising, and presents the plain's provisions to wetlands as due to the extreme moisture contents during the summer in the year 2010. In general, the flood events turn to normality on 8 October 2010, from beginning to end in the broad picture over the region. The overall results indicate that the monsoon's heavy rain or flood during the summer does not affect the winter crop over the plain of Punjab, Pakistan. Overall, this indicates that the monsoon's heavy rain and flood affected the region, and presents significant outcomes of the natural hazards associated with climate extremes during the year 2010. Based on the Pakistan Bureau of Statistics, these findings illustrate that, during the 12 years of the winter wheat crop seasons, in the years 2004, 2006, 2008, 2010, and 2011, the decrease was calculated with 2500, 2588, 2438, 2846, and 2737 yield per hectare in kgs, from the average yield production under both rain-fed and irrigated conditions in the plain. Before and after the flood inception, the wheat crop area was 6691.0 hectares in 2010–2011, whereas, in 2011–2012, it decreased to 6482.9 hectares. This shows that the flood (2010) affected the area and the production, and decreased from 19.041 to 17.7389 million tons. With regards to the abovementioned drought and yield calculations, it is illustrated that there are insufficient irrigated practices in the plain and a reliance on the seasonal drought and flood events during the winter wheat crop season in the plain of Punjab.

Generally, the study's achievable goals and advice are applicable to the climate change threats towards Asia and are specific to the region (e.g., Dai [30,32] and Wu et al. [60]), with respect to temperature extremes, glacier melts, flooding, and drought conditions. This knowledge highlights the problem of climate change, with a focus on natural disasters, and urges policymakers to recognize the extreme vulnerability and impacts of temperature changes, heat extremes, heavy rain falls, glacier melts, river/stream flow, and agriculture on the region of Pakistan.

Author Contributions: Conceptualization, J.K. and R.U.; methodology, R.U.; software, J.K.; validation, J.K., R.U. and I.U.; formal analysis, I.U.; investigation, R.U.; resources, J.K.; data curation, J.K.;

writing—original draft preparation, R.U.; writing—review and editing, I.U.; visualization, R.U.; supervision, R.U.; project administration, F.K. and Y.L.; funding acquisition, F.K.; Y.L. All authors have read and agreed to the published version of the manuscript.

Funding: This This work was supported in part by the National Research Foundation of Korea (NRF) grant 2022R1G1A1003531 and Institute of Information & communications Technology Planning & Evaluation (IITP) grant IITP-2022-2020-0-101741, RS-2022-00155885 funded by the Korea government (MSIT).

Data Availability Statement: Not applicable.

Conflicts of Interest: The authors declare no conflict of interest.

References

1. Wilhite, D.; Svoboda, M.; Hayes, M. Understanding the complex impacts of drought: A key to enhancing drought mitigation and preparedness. *Water Resour. Manag.* **2007**, *21*, 763–774. <https://doi.org/10.1007/s11269-006-9076-5>.
2. Wu, J.; Chen, X.; Love, C.A.; Yao, H.; Chen, X.; AghaKouchak, A. Determination of water required to recover from hydrological drought: Perspective from drought propagation and non-standardized indices. *J. Hydrol.* **2020**, *590*, 125227. <https://doi.org/10.1016/j.jhydrol.2020.125227>.
3. Ullah, I.; Ma, X.; Yin, J.; Asfaw, T.G.; Azam, K.; Syed, S.; Liu, M.; Arshad, M.; Shahzaman, M. Evaluating the meteorological drought characteristics over Pakistan using in situ observations and reanalysis products. *Int. J. Climatol.* **2021**, *41*, 4437–4459. <https://doi.org/10.1002/joc.7063>.
4. Hina, S.; Saleem, F.; Arshad, A.; Hina, A.; Ullah, I. Droughts over Pakistan: possible cycles, precursors and associated mechanisms. *Geomat. Nat. Hazards Risk* **2021**, *12*, 1638–1668. <https://doi.org/10.1080/19475705.2021.1938703>.
5. Shahzaman, M.; Zhu, W.; Ullah, I.; Mustafa, F.; Bilal, M.; Ishfaq, S.; Nisar, S.; Arshad, M.; Iqbal, R.; Aslam, R.W. Comparison of multi-year reanalysis, models, and satellite remote sensing products for agricultural drought monitoring over South Asian countries. *Remote Sens.* **2021**, *13*, 3294. <https://doi.org/10.3390/rs13163294>.
6. Ullah, I.; Ma, X.; Yin, J.; Saleem, F.; Syed, S.; Omer, A.; Habtemicheal, B.A.; Liu, M.; Arshad, M. Observed changes in seasonal drought characteristics and their possible potential drivers over Pakistan. *Int. J. Climatol.* **2022**, *42*, 1576–1596. <https://doi.org/10.1002/joc.7321>.
7. Sein, Z.M.M.; Zhi, X.; Ullah, I.; Azam, K.; Ngoma, H.; Saleem, F.; Xing, Y.; Iyakaremye, V.; Syed, S.; Hina, S.; et al. Recent variability of sub-seasonal monsoon precipitation and its potential drivers in Myanmar using in-situ observation during 1981–2020. *Int. J. Climatol.* **2022**, *42*, 3341–3359. <https://doi.org/10.1002/joc.7419>.
8. Ahmad, B.; Kaleem, M.S.; Butt, M.J.; Dahri, Z.H. Hydrological modelling and flood hazard mapping of Nullah Lai. *Proc. Pakistan Acad. Sci.* **2010**, *47*, 215–226.
9. Shahzaman, M.; Zhu, W.; Bilal, M.; Habtemicheal, B.; Mustafa, F.; Arshad, M.; Ullah, I.; Ishfaq, S.; Iqbal, R. Remote sensing indices for spatial monitoring of agricultural drought in South Asian countries. *Remote Sens.* **2021**, *13*, 2059. <https://doi.org/10.3390/rs13112059>.
10. Arshad, M.; Ma, X.; Yin, J.; Ullah, W.; Liu, M.; Ullah, I. Performance evaluation of ERA-5, JRA-55, MERRA-2, and CFS-2 reanalysis datasets, over diverse climate regions of Pakistan. *Weather Clim. Extrem.* **2021**, *33*, 100373. <https://doi.org/10.1016/j.wace.2021.100373>.
11. Ullah, I.; Saleem, F.; Iyakaremye, V.; Yin, J.; Ma, X.; Syed, S.; Hina, S.; Asfaw, T.G.; Omer, A. Projected changes in socioeconomic exposure to heatwaves in South Asia under changing climate. *Earth's Future* **2022**, *10*, e2021EF002240. <https://doi.org/10.1029/2021EF002240>.
12. Uwimbabazi, J.; Jing, Y.; Iyakaremye, V.; Ullah, I.; Ayugi, B. Observed changes in meteorological drought events during 1981–2020 over Rwanda, East Africa. *Sustainability* **2022**, *14*, 1519. <https://doi.org/10.3390/su14031519>.
13. Lu, K.; Arshad, M.; Ma, X.; Ullah, I.; Wang, J.; Shao, W. Evaluating observed and future spatiotemporal changes in precipitation and temperature across China based on CMIP6-GCMs. *Int. J. Climatol.* **2022**, *42*, 7703–7729. <https://doi.org/10.1002/joc.7673>.
14. Sajjad, M.M.; Wang, J.; Abbas, H.; Ullah, I.; Khan, R.; Ali, F. Impact of climate and land-use change on groundwater resources, study of Faisalabad District, Pakistan. *Atmosphere* **2022**, *13*, 1097. <https://doi.org/10.3390/atmos13071097>.
15. Ahmad, Z.; Hafeez, M.; Ahmad, I. Hydrology of mountainous areas in the upper Indus Basin, Northern Pakistan with the perspective of climate change. *Environ. Monit. Assess.* **2012**, *184*, 5255–5274. <https://doi.org/10.1007/s10661-011-2337-7>.
16. Hassan, M.; Du, P.; Mahmood, R.; Jia, S.; Iqbal, W. Streamflow response to projected climate changes in the Northwestern Upper Indus Basin based on regional climate model (RegCM4.3) simulation. *J. Hydro-Environment Res.* **2019**, *27*, 32–49. <https://doi.org/10.1016/j.jher.2019.08.002>.
17. Ullah, I.; Ma, X.; Asfaw, T.G.; Yin, J.; Iyakaremye, V.; Saleem, F.; Xing, Y.; Azam, K.; Syed, S. Projected changes in increased drought risks over South Asia under a warmer climate. *Earth's Future* **2022**, *10*, e2022EF002830. <https://doi.org/10.1029/2022EF002830>.
18. Xing, Y.; Shao, D.; Liang, Q.; Chen, H.; Ma, X.; Ullah, I. Investigation of the drainage loss effects with a street view based drainage calculation method in hydrodynamic modelling of pluvial floods in urbanized area. *J. Hydrol.* **2022**, *605*, 127365. <https://doi.org/10.1016/j.jhydrol.2021.127365>.

19. Sein, Z.M.M.; Ullah, I.; Iyakaremye, V.; Azam, K.; Ma, X.; Syed, S.; Zhi, X. Observed spatiotemporal changes in air temperature, dew point temperature and relative humidity over Myanmar during 2001–2019. *Meteorol. Atmos. Phys.* **2022**, *134*, 7. <https://doi.org/10.1007/s00703-021-00837-7>.
20. Ullah, I.; Ma, X.; Yin, J.; Omer, A.; Habtemicheal, B.A.; Saleem, F.; Iyakaremye, V.; Syed, S.; Arshad, M.; Liu, M. Spatiotemporal characteristics of meteorological drought variability and trends (1981–2020) over South Asia and the associated large-scale circulation patterns. *Clim. Dyn.* **2022**. <https://doi.org/10.1007/s00382-022-06443-6>.
21. Mie Sein, Z.M.; Ullah, I.; Saleem, F.; Zhi, X.; Syed, S.; Azam, K. Interdecadal variability in myanmar rainfall in the Monsoon Season (May–October) using eigen methods. *Water* **2021**, *13*, 729. <https://doi.org/10.3390/w13050729>.
22. Ullah, I.; Ma, X.; Ren, G.; Yin, J.; Iyakaremye, V.; Syed, S.; Lu, K.; Xing, Y.; Singh, V.P. Recent changes in drought events over South Asia and their possible linkages with climatic and dynamic factors. *Remote Sens.* **2022**, *14*, 3219. <https://doi.org/10.3390/rs14133219>.
23. Aadhar, S.; Mishra, V. A substantial rise in the area and population affected by dryness in South Asia under 1.5 °C, 2.0 °C and 2.5 °C warmer worlds. *Environ. Res. Lett.* **2019**, *14*, 114021. <https://doi.org/10.1088/1748-9326/ab4862>.
24. Zhou, J.; Jiang, T.; Wang, Y.; Su, B.; Tao, H.; Qin, J.; Zhai, J. Spatiotemporal variations of aridity index over the Belt and Road region under the 1.5 °C and 2.0 °C warming scenarios. *J. Geogr. Sci.* **2020**, *30*, 37–52. <https://doi.org/10.1007/s11442-020-1713-z>.
25. Wu, J.; Yuan, X.; Yao, H.; Chen, X.; Wang, G. Reservoirs regulate the relationship between hydrological drought recovery water and drought characteristics. *J. Hydrol.* **2021**, *603*, 127127. <https://doi.org/10.1016/j.jhydrol.2021.127127>.
26. Ali, S.; Xu, Z.T.; Henchirli, M.; Wilson, K.; Zhang, J. Studying of drought phenomena and vegetation trends over South Asia from 1990 to 2015 by using AVHRR and NASA’s MERRA data. *Environ. Sci. Pollut. Res.* **2020**, *27*, 4756–4768. <https://doi.org/10.1007/s11356-019-07221-4>.
27. Ullah, R.; Khan, J.; Ullah, I.; Khan, F.; Lee, Y. Assessing impacts of flood and drought over the Punjab Region of Pakistan using multi-satellite data products. *Remote Sens.* **2023**, *15*, 1484. <https://doi.org/10.3390/rs15061484>.
28. Palmer, W.C. *Meteorological Drought*; Pap. No. 45; US Department of Commerce, Weather Bureau: Washington, DC, USA, 1965; 58p.
29. McKee, T.B.; Nolan, J.; Kleist, J. The relationship of drought frequency and duration to time scales. In Proceedings of the 8th Conference on Applied Climatology, Anaheim, CA, USA, 17–22 January 1993.
30. Dai, A. Hydroclimatic trends during 1950–2018 over global land. *Clim. Dyn.* **2021**, *56*, 4027–4049. <https://doi.org/10.1007/s00382-021-05684-1>.
31. Liu, M.; Ma, X.; Yin, Y.; Zhang, Z.; Yin, J.; Ullah, I.; Arshad, M. Non-stationary frequency analysis of extreme streamflow disturbance in a typical ecological function reserve of China under a changing climate. *Ecohydrology* **2021**, *23*, e2323. <https://doi.org/10.1002/eco.2323>.
32. Dai, A. Characteristics and trends in various forms of the Palmer Drought Severity Index during 1900–2008. *J. Geophys. Res. Atmos.* **2011**, *116*. <https://doi.org/10.1029/2010JD015541>.
33. Dai, A. Increasing drought under global warming in observations and models. *Nat. Clim. Change* **2013**, *3*, 52–58. <https://doi.org/10.1038/nclimate1633>.
34. Wu, J.; Chen, X.; Yao, H.; Gao, L.; Chen, Y.; Liu, M. Non-linear relationship of hydrological drought responding to meteorological drought and impact of a large reservoir. *J. Hydrol.* **2017**, *551*, 495–507. <https://doi.org/10.1016/j.jhydrol.2017.06.029>.
35. Bowling, L.C.; Lettenmaier, D.P.; Nijssen, B.; Graham, L.P.; Clark, D.B.; El Maayar, M.; Essery, R.; Goers, S.; Gusev, Y.M.; Habets, F.; et al. Simulation of high-latitude hydrological processes in the Torne-Kalix basin: PILPS Phase 2(e) 1: Experiment description and summary intercomparisons. *Glob. Planet. Change* **2003**, *38*, 1–30. [https://doi.org/10.1016/S0921-8181\(03\)00003-1](https://doi.org/10.1016/S0921-8181(03)00003-1).
36. Ferrant, S.; Bustillo, V.; Burel, E.; Salmon-Monviola, J.; Claverie, M.; Jarosz, N.; Yin, T.; Rivalland, V.; Dedieu, G.; Demarez, V.; et al. Extracting soil water holding capacity parameters of a distributed agro-hydrological model from high resolution optical satellite observations series. *Remote Sens.* **2016**, *8*, 154. <https://doi.org/10.3390/rs8020154>.
37. Tanaka, M.; Sugimura, T.; Tanaka, S.; Tamai, N. Flood–drought cycle of Tonle Sap and Mekong Delta area observed by DMSP-SSM/I. *Int. J. Remote Sens.* **2003**, *24*, 1487–1504. <https://doi.org/10.1080/01431160110070726>.
38. Ali, M.; Ghaith, M.; Wagdy, A.; Helmi, A.M. Development of a new multivariate composite drought index for the Blue Nile River Basin. *Water* **2022**, *14*, 886. <https://doi.org/10.3390/w14060886>.
39. Iyakaremye, V.; Zeng, G.; Yang, X.; Zhang, G.; Ullah, I.; Gahigi, A.; Vuguziga, F.; Asfaw, T.; Ayugi, B. Increased high-temperature extremes and associated population exposure in Africa by the mid-21st century. *Sci. Total Environ.* **2021**, *790*, 148162. <https://doi.org/10.1016/j.scitotenv.2021.148162>.
40. Iyakaremye, V.; Zeng, G.; Ullah, I.; Gahigi, A.; Mumo, R.; Ayugi, B. Recent observed changes in extreme high-temperature events and associated meteorological conditions over Africa. *Int. J. Climatol.* **2022**, *42*, 4522–4537. <https://doi.org/10.1002/joc.7485>.
41. Mie Sein, Z.; Ullah, I.; Syed, S.; Zhi, X.; Azam, K.; Rasool, G. Interannual variability of air temperature over Myanmar: The influence of ENSO and IOD. *Climate* **2021**, *9*, 35. <https://doi.org/10.3390/cli9020035>.
42. Han, Y.; Wang, Y.; Zhao, Y. Estimating soil moisture conditions of the greater Changbai Mountains by land surface temperature and NDVI. *IEEE Trans. Geosci. Remote Sens.* **2010**, *48*, 2509–2515. <https://doi.org/10.1109/TGRS.2010.2040830>.
43. Ahmed, K.; Shahid, S.; Wang, X.; Nawaz, N.; Khan, N. Spatiotemporal changes in aridity of Pakistan during 1901–2016. *Hydrol. Earth Syst. Sci.* **2019**, *23*, 3081–3096. <https://doi.org/10.5194/hess-23-3081-2019>.
44. Arshad, M.; Ma, X.; Yin, J.; Ullah, W.; Ali, G.; Ullah, S.; Liu, M.; Shahzaman, M.; Ullah, I. Evaluation of GPM-IMERG and TRMM-3B42 precipitation products over Pakistan. *Atmos. Res.* **2021**, *249*, 105341. <https://doi.org/10.1016/j.atmosres.2020.105341>.

45. Yuan, Y.F.; Zhai, P.M.; Li, J.; Chen, Y. Changes in classified precipitation in the urban, suburban, and mountain areas of Beijing. *Adv. Clim. Change Res.* **2017**, *8*, 279–285. <https://doi.org/10.1016/j.accre.2017.10.002>.
46. Harris, I.; Osborn, T.J.; Jones, P.; Lister, D. Version 4 of the CRU TS monthly high-resolution gridded multivariate climate dataset. *Sci. Data* **2020**, *7*, 109. <https://doi.org/10.1038/s41597-020-0453-3>.
47. Wu, J.; Zhou, L.; Mo, X.; Zhou, H.; Zhang, J.; Jia, R. Drought monitoring and analysis in China based on the Integrated Surface Drought Index (ISDI). *Int. J. Appl. Earth Obs. Geoinf.* **2015**, *41*, 23–33. <https://doi.org/10.1016/j.jag.2015.04.006>.
48. Kulkarni, S.S.; Wardlow, B.D.; Bayissa, Y.A.; Tadesse, T.; Svoboda, M.D.; Gedam, S.S. Developing a remote sensing-based combined drought indicator approach for agricultural drought monitoring over Marathwada, India. *Remote Sens.* **2020**, *12*, 2091. <https://doi.org/10.3390/rs12132091>.
49. Tabassum, R.; Arsalan, M.H.; Khalid, A.; Ahmad, I.; Mirza, A.I.; Abad, S.B. Assessment of drought risk by using vegetation indices from remotely sensed data: A perspective from hot and arid district of Pakistan. *Univ. Eng. Technol. Taxila. Tech. J.* **2015**, *20*, 2–7.
50. Prakash, S. Performance assessment of CHIRPS, MSWEP, SM2RAIN-CCI, and TMPA precipitation products across India. *J. Hydrol.* **2019**, *571*, 50–59. <https://doi.org/10.1016/j.jhydrol.2019.01.036>.
51. Sadegh, M.; Ragno, E.; AghaKouchak, A. Multivariate Copula Analysis Toolbox (MvCAT): Describing dependence and underlying uncertainty using a Bayesian framework. *Water Resour. Res.* **2017**, *53*, 5166–5183. <https://doi.org/10.1002/2016WR020242>.
52. Wan, Z.; Wang, P.; Li, X. Using MODIS land surface temperature and normalized difference vegetation index products for monitoring drought in the southern Great Plains, USA. *Int. J. Remote Sens.* **2004**, *25*, 61–72. <https://doi.org/10.1080/0143116031000115328>.
53. Sun, W.; Wang, P.-X.; Zhang, S.-Y.; Zhu, D.-H.; Liu, J.-M.; Chen, J.-H.; Yang, H.-S. Using the vegetation temperature condition index for time series drought occurrence monitoring in the Guanzhong Plain, PR China. *Int. J. Remote Sens.* **2008**, *29*, 5133–5144. <https://doi.org/10.1080/01431160802036557>.
54. Tian, M.; Wang, P.; Khan, J. Drought forecasting with vegetation temperature condition index using ARIMA models in the Guanzhong Plain. *Remote Sens.* **2016**, *8*, 690. <https://doi.org/10.3390/rs8090690>.
55. Zeng, X.; Lu, E. Globally unified monsoon onset and retreat indexes. *J. Clim.* **2004**, *17*, 2241–2248. [https://doi.org/10.1175/1520-0442\(2004\)017<2241:GUMOAR>2.0.CO;2](https://doi.org/10.1175/1520-0442(2004)017<2241:GUMOAR>2.0.CO;2).
56. Adnan, S.; Ullah, K.; Shouting, G. Investigations into precipitation and drought climatologies in south central Asia with special focus on Pakistan over the period 1951–2010. *J. Clim.* **2016**, *29*, 6019–6035. <https://doi.org/10.1175/JCLI-D-15-0735.1>.
57. Liang, M.; Yuan, X. Critical role of soil moisture memory in predicting the 2012 Central United States flash drought. *Front. Earth Sci.* **2021**, *9*, 615969. <https://doi.org/10.3389/feart.2021.615969>.
58. Wu, J.; Chen, X.; Yu, Z.; Yao, H.; Li, W.; Zhang, D. Assessing the impact of human regulations on hydrological drought development and recovery based on a ‘simulated-observed’ comparison of the SWAT model. *J. Hydrol.* **2019**, *577*, 123990. <https://doi.org/10.1016/j.jhydrol.2019.123990>.
59. Wu, Z.; Huang, N.E.; Wallace, J.M.; Smoliak, B.V.; Chen, X. On the time-varying trend in global-mean surface temperature. *Clim. Dyn.* **2011**, *37*, 759. <https://doi.org/10.1007/s00382-011-1128-8>.
60. Wu, J.; Chen, X. Spatiotemporal trends of dryness/wetness duration and severity: The respective contribution of precipitation and temperature. *Atmos. Res.* **2019**, *216*, 176–185. <https://doi.org/10.1016/j.atmosres.2018.10.005>.

Disclaimer/Publisher’s Note: The statements, opinions and data contained in all publications are solely those of the individual author(s) and contributor(s) and not of MDPI and/or the editor(s). MDPI and/or the editor(s) disclaim responsibility for any injury to people or property resulting from any ideas, methods, instructions or products referred to in the content.